

University of Colorado  
 Department of Aerospace Engineering Sciences  
 Senior Projects - ASEN 4018  
 Conceptual Design Document (CDD)

## Mapping Architecture Concept for Universal Landing Automation (MACULA)

### Approvals

	Name	Affiliation	Approved	Date
Course Coordinator	James Nability	CU AES		

### Project Customers

Jeffrey Thayer Department of Aerospace Engineering Sciences University of Colorado at Boulder Boulder, CO 80309 Phone: (303) 492-1764 Email: Jeffrey.Thayer@Colorado.edu	Brian Argrow Department of Aerospace Engineering Sciences University of Colorado at Boulder Boulder, CO 80309 Phone: (303) 492-5312 Email: Brian.Argrow@Colorado.edu
---	---

### Team Members

<b>Arrasmith, Trevor</b> (Software Lead) Trevor.Arrasmith@Colorado.edu (720) 301-0237	<b>Bender, Brett</b> (Mechanical Lead) Brett.Bender@Colorado.edu (440) 488-3321
<b>Brown, Christopher</b> (Manufacturing Lead) Christopher.J.Brown@Colorado.edu (970) 485-9381	<b>Dawson, Nicholas</b> (Financial Officer) nickdawson95@gmail.com (303) 667-4761
<b>Emmert, David</b> (Systems Engineer) David.Emmert@Colorado.edu (815) 762-1460	<b>Garby, Bryce</b> (Electrical Lead) Bryce.Garby@Colorado.edu (303) 570-8276
<b>Gleason, Russell</b> (Safety Officer) Russell.Gleason@Colorado.edu (425) 281-0805	<b>Hurst, Matthew</b> (Project Manager) Matthew.R.Hurst@Colorado.edu (303) 506-0501
<b>Levin, Jared</b> (Test Engineer) Jared.Levin@Colorado.edu (720) 381-9993	<b>Rothstein-Dowden, Ansel</b> (Modeling Lead) Ansel.Rothsteindowden@Colorado.edu (774) 392-4555

# Contents

<b>1</b>	<b>Project Description</b>	<b>5</b>
1.1	Purpose . . . . .	5
1.2	Project Objectives . . . . .	5
1.3	Concept of Operations . . . . .	6
1.4	Functional Block Diagram . . . . .	7
1.5	Functional Requirements . . . . .	8
<b>2</b>	<b>Design Requirements</b>	<b>9</b>
<b>3</b>	<b>Key Design Options Considered</b>	<b>15</b>
3.1	Lidar Sensor . . . . .	15
3.1.1	Building a Lidar . . . . .	15
3.1.2	Fixed-Beam Lidar . . . . .	16
3.1.3	Multiple Fixed-Beam Lidars . . . . .	17
3.1.4	Scanning Lidar . . . . .	17
3.1.5	Optically Segmented Lidar . . . . .	18
3.1.6	Flash Lidar . . . . .	19
3.2	Scanning Mechanism . . . . .	20
3.2.1	Mechanical System . . . . .	20
3.2.2	Risley Prisms . . . . .	21
3.2.3	Optical Mirrors . . . . .	22
3.2.4	Translational Mechanical Scanning System . . . . .	24
3.3	Hazard Detection Algorithm . . . . .	26
3.3.1	Smoothing Techniques . . . . .	26
3.3.1.1	Nodal Surface Approximation . . . . .	26
3.3.1.2	Modal Surface Approximation . . . . .	27
3.3.2	Gradient-Based Techniques . . . . .	27
3.3.2.1	Morphological Filter . . . . .	27
3.3.2.2	Kernel Convolution Filter . . . . .	28
3.3.2.3	Displaced Points Method . . . . .	28
<b>4</b>	<b>Trade Study Process and Results</b>	<b>30</b>
4.1	Lidar Selection . . . . .	30
4.1.1	Criteria and Weighting . . . . .	30
4.1.2	Trade Study Scoring . . . . .	31
4.1.3	Trade Study . . . . .	32
4.2	Scanning System Selection . . . . .	33
4.2.1	Criteria and Weighting . . . . .	33
4.2.2	Trade Study Scoring . . . . .	35
4.2.3	Trade Study . . . . .	35
4.2.4	Mirror/Gimbal Hybrid . . . . .	37
4.2.5	Trade Study with Mirror/Gimbal Hybrid . . . . .	38
4.3	Software Selection . . . . .	38
4.3.1	Criteria, Weighting, and Scoring . . . . .	38
4.3.2	Trade Study . . . . .	40
<b>5</b>	<b>Selection of Baseline Design</b>	<b>40</b>
	<b>Appendix</b>	<b>44</b>

<b>A</b>	<b>Deriving Allowable Angular Position Uncertainty</b>	<b>44</b>
A.1	Setting the Scene . . . . .	44
A.2	Deriving the Governing Equations . . . . .	44
A.3	Special Cases . . . . .	46
A.4	Applying the Mathematics to the Conceptual Design . . . . .	46
<b>B</b>	<b>Translation of Range and Angular Position Information to Points in Inertial Space</b>	<b>48</b>
B.1	Overview . . . . .	48
B.2	Factors Leading to a More Complex Transformation than Spherical to Cartesian Coordinate Frames . . . . .	48
B.3	Pitch Plate Geometry . . . . .	48
B.3.1	Vectorized Geometry . . . . .	49
B.4	Definition of Co-rotating Frames . . . . .	50
B.5	Derivation of Governing Equation . . . . .	50
<b>C</b>	<b>Hazard Detection and Definition</b>	<b>52</b>
C.1	Shadowing . . . . .	52
C.2	Maximum Scan Angle . . . . .	52
C.3	Hazard Definition . . . . .	53
<b>D</b>	<b>Stroking Neighbor Method</b>	<b>58</b>
<b>E</b>	<b>Algorithm Unit Test Maps</b>	<b>60</b>
<b>F</b>	<b>Required Sample Rate Derivation</b>	<b>62</b>

## Nomenclature

### Acronyms and Abbreviations

CONOPS	Concept of Operations
COTS	Commercial Off The Shelf
CPU	Central Processing Unit
CU	University of Colorado at Boulder
DAQ	Data Acquisition System
DR	Design Requirement
EDL	Entry, Descent, and Landing
FR	Functional Requirement
GPIO	General Purpose In/Out (Pin)
IMU	Inertial Measurement Unit
LIDAR (lidar)	Light Detection and Ranging
MACULA	Mapping Architecture Concept for Universal Landing Automation
NURBS	Non-Uniform Rational Basis Spline
PC	Personal Computer
TRL	Technology Readiness Level

### Symbols

$\alpha$	Angular acceleration
$\tau$	Torque
$I$	Moment of inertia
$AR_s$	Aspect ratio of rock from a side view
$AR_t$	Aspect ratio of rock from a top view
$\delta$	Angular change
$h$	Height of rock
$l$	Length of rock
$w$	Width of rock

# 1 Project Description

## 1.1 Purpose

**G**UIDED landing of modern spacecraft is often limited in accuracy and application. The inability of a spacecraft to dynamically scan unknown terrain limits potential landing sites to preselected zones with minimal hazards. Additionally, the uncertainty in the trajectory of the craft during landing requires that these preselected zones be orders of magnitude larger than the craft itself in order to achieve the desired levels of safety. This results in landing zones that are often far from areas of scientific interest, such as craters or places of high geological variety.

Not only are landing craft limited to these safe zones, but this method requires detailed prior knowledge of the target body's terrain. In cases such as Mars, this is a viable option given the detailed surface mapping that has been obtained from imaging spacecraft in orbit around the planet. However, utilizing this approach for other celestial bodies is less viable because it would require multiple missions or additional orbital maneuvers in order to create a sufficiently detailed map before being able to safely land on the body.

Having the ability to dynamically detect and avoid obstacles on landing would create new avenues for scientific research by allowing these craft to land in areas that would otherwise be too hazardous. This would increase the scientific productivity of rovers by cutting out extensive travel periods that are both expensive to operate and physically damaging to the rover. Used in conjunction with propulsive landing, this mapping system provides a distinct improvement to the entry, descent, and landing (EDL) phase of missions to other celestial bodies. Applied to the Mars Curiosity rover, this system could have removed the need for miles of travel on the path to Mount Sharp. Applied to future systems, landers and rovers can be placed more strategically, possibly even removing the need for mobile vehicles on some missions.

The MACULA\* project is presented by the CU Aerospace Engineering department. Its purpose is to design, manufacture, and test a proof-of-concept light detection and ranging (lidar) scanning system for a landing craft. Since the project is a proof of concept, strict mass and size requirements are not enforced. The scanning system will create a three-dimensional point cloud representing the scanned terrain. This point cloud will then be analyzed by on-board software to detect hazards and select a safe landing zone.

This document will detail the conceptual design process, including key design options and trade studies. Several appendices have been included, which are not necessary for a complete report but provide justification for many components of the analysis.

## 1.2 Project Objectives

The success levels shown below in Table 1 categorize the high-level objectives that must be completed to build, validate, and verify a lidar-based dynamic hazard detection and avoidance system. Level 1 success will be met if the system hardware is built, integrated, and capable of producing a point cloud in three dimensions. This will include the basic software development required for all subsystems to operate and communicate automatically after high-level user commands have been given. Additionally, Level 1 success must validate the mapping model by recording measurements at the range and spatial resolution specified in Table 1. Completion of Level 1 success will result in a physical system that can be used to implement and test hazard detection and avoidance algorithms. All further levels of success must build on previous levels, in that the success of any given level must also meet the success requirements of all previous levels. Levels 2 through 4 are concerned with development of a hazard detection and landing location selection algorithm, and the mock-up scene required to test it. Level 4 success defines the overall design goal of the project.

---

\*The macula is the part of the eye with the greatest visual acuity.

Table 1: MACULA Project Success Levels

Level	Hardware: Lidar Scanning System	Software Development	Test Bed
1	Lidar sensor and scanning system shall obtain measurements with a 0.1m spatial resolution at a 14.1m*range and a maximum angle of 20° from nadir	Subsystems shall interact to record and output correlated range and attitude measurements	Stationary platform shall be built to house and operate the lidar scanning system
2	Scanning process shall be completed in less than 60 seconds	Range and attitude measurements with uncertainties shall be projected into a three-dimensional point cloud within the same 60-second time requirement as the hardware scan	Arbitrary test scene with dimensions known to an accuracy better than 0.01m shall be scanned with lidar in order to verify mapping accuracy
3	-	Topographic map shall be analyzed to create a map of hazards, within the same 60-second requirement	Landing zone mock-up with known hazards shall be constructed with dimensions known to an accuracy better than 0.01m in order to verify hazard detection
4	-	Within the same 60-seconds, hazard map shall be analyzed to determine the nearest safe landing zone; if no safe zones are detected, hazard definitions will be loosened until the first viable landing zone is detected	-

### 1.3 Concept of Operations

During conventional EDL operations, landing craft will execute a short hover phase where horizontal and vertical velocities become approximately zero. Within the scope of the MACULA project, all mission objectives are to be completed during this phase so that the system may be mounted for stationary testing.

To begin, both the lidar sensor and scanning system will be activated to scan the terrain. Range and attitude measurements from the lidar and scanning system will be used to construct a point cloud where obstacles and regions of high gradient will be detected. With each point of measurement being qualified as safe or unsafe the algorithm will choose the closest suitably large safe area as a landing site. Note that the operations described in Fig. 1 would achieve all four levels of success.

\*This requirement will be described later in the document.

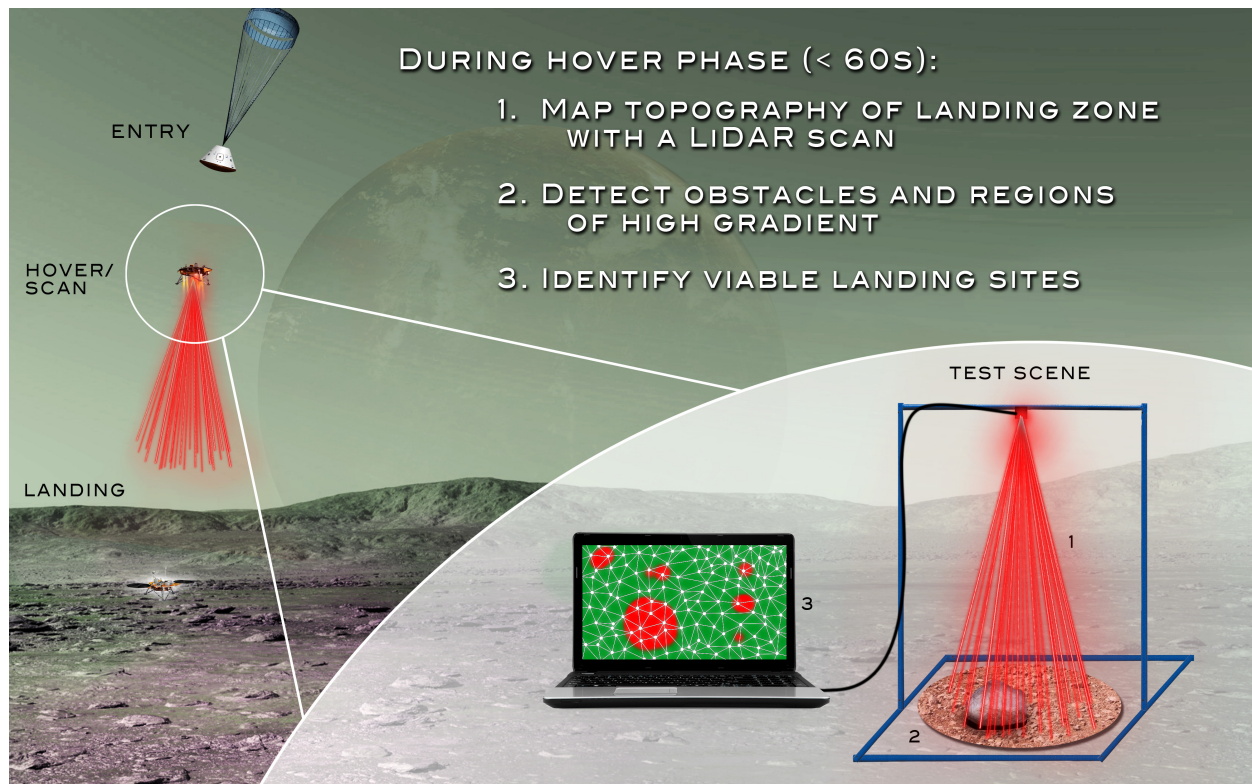


**Figure 1: MACULA Concept of Operations (CONOPS)**

## 1.4 Functional Block Diagram

The underlying structure of the project can be broken down into four distinct components: a personal computer (PC) interface, an on-board Central Processing Unit (CPU), the sensor package\*, and the test bed. These four components are shown in the functional block diagram (FBD) in Fig. 2 below.

The process begins when the PC commands the system to initiate operation. A scan pattern algorithm contained within the on-board CPU will then send instructions to the controller, which will in turn command one or more actuators to manipulate the lidar beam direction. Range measurements from the lidar and attitude measurements from the sensor package will then be delivered into the Data Acquisition System (DAQ) along with simulated IMU data from the PC. This unit may exist on-board the CPU or may be separate. Raw sensor data is processed on the DAQ into a machine-readable format. Processed data will be used to construct the required topographic map, and hazards existing within the map will be detected. With a map of landing hazards constructed, the algorithm can then select a safe landing zone for the craft. If no landing zone is found, the map will be re-analyzed with looser tolerances until one is found. With a selected landing site, information from the on-board processor containing all stages of the analysis will be transferred to and displayed on the PC, where additional analysis will be done for visual confirmation of the point cloud construction and hazard detection.

\*The sensor package, as defined later, is made up of the scanning system, the lidar, and any other necessary components for obtaining measurements.

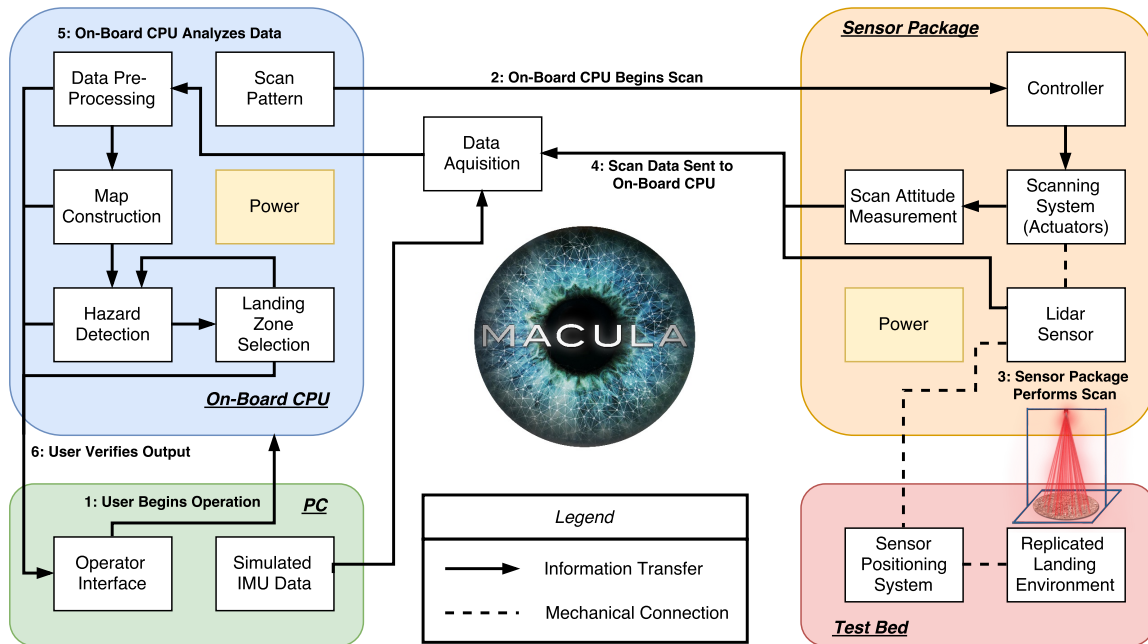


Figure 2: MACULA Functional Block Diagram

### 1.5 Functional Requirements

The project functional requirements are summarized in Table 2. These functional requirements will be described in more detail in the next section.

Table 2: MACULA Functional Requirements

1	The system shall implement a proof-of-concept landing assist system for a CubeSat lander.
2	The on-board processor shall receive commands and data from a user-operated PC.
3	The on-board processor shall command the sensor package.
4	The sensor package shall utilize lidar to obtain range measurements at known orientations.
5	The sensor package shall transmit data to an on-board processor or DAQ.
6	The on board processor shall translate the range and attitude data into a three-dimensional point cloud.
7	The on-board processor shall analyze the 3D point cloud for hazards.
8	The on-board processor shall select an acceptable landing site.
9	The system shall generate output readable by the PC.

## 2 Design Requirements

**FR 1** The system shall implement a proof-of-concept landing assist system for a CubeSat lander.

*Motivation:* Large scale aerospace projects produced by companies such as NASA or SpaceX tend to have very large budgets, with significant financial consequences if the mission should fail. One such example is the NASA Curiosity Rover, which is estimated to have cost \$2.5 billion<sup>6</sup>. As a result, these high-profile projects have the economic means and motivations to purchase or develop highly effective landing architectures. Alternatively, CubeSat projects can be estimated to cost in the range of \$500,000 to \$1 million, as quoted by Blue Canyon Technologies. The lower budget of these systems puts significant limits on the types of hardware and subsystems that can be implemented in the project. With a budget of \$5,000, the dynamic scanning system concept proposed by this project would demonstrate the capabilities of a low-cost lidar scanning system, which would provide significant benefits to CubeSat landing projects.

**DR 1.1** The system shall be capable of scanning terrain in two dimensions, centered in the nadir direction.

- *Motivation:* In order to direct the landing craft to an acceptable (**DR 7.1**) landing location, the system must obtain ground height data over a two-dimensional space containing an area in which the craft can change its direction and land.
- *Verification:* The scanning system can be visually confirmed to scan in two dimensions.

**DR 1.2** The system shall have a maximum scan angle of 20° off of nadir.

- *Motivation:* The system must have a maximum scan angle sufficiently large that the area of the scanned ground provides a suitable number of landing sites\*. The effect of shadowing as explained in Appendix C.1 should also not dominate the spacing of the scanned points. The balance between these driving factors is explained in Appendix C.2.
- *Verification:* The scan angle can be verified by confirming that the system can actuate the beam to an angle of 20° off of nadir. This can be demonstrated by mounting the system on an optics bench and sending visible light through the scanning system, measuring the beam location within the optics bench and translating this into the scan angle.

**DR 1.3** The scan target area shall be located at a nadir range of 14.1m.

- *Motivation:* The customer has provided a range requirement of 15m. This range requirement has been taken as the slant range<sup>†</sup> Using 15m as the slant range and 20° as the scan angle results in a nadir range of 14.1m.
- *Verification:* The distance between the lidar scanner and the test mock-up ground plane will be manually measured using a tape measure.

**DR 1.4** The distance between scanned points shall be less than or equal to 0.1m.

- *Motivation:* Statistical analysis of rocks on Mars (a characteristically rocky landing location) has shown that a scan resolution of 0.1m yields a 1.1% chance of a hazardous obstacle going undetected by the scan. See Appendix C.3 for further information.
- *Verification:* The scan angle measurements can be mathematically projected onto a plane at 14.1m away from the scan source, and the spatial resolution can be calculated from these points as the average distance to the closest neighboring point.

**DR 1.5** The system shall complete the scan and analysis in under 60 seconds.

- *Motivation:* This time constraint is a customer requirement. In a mission scenario, the system must scan the ground and select a suitable landing zone within an amount of time specified by the CubeSat lander propulsive hover capabilities.
- *Verification:* This will be a full-system validation test in which the scan and analysis are performed within the time requirement, confirmed by external time measurements.

**FR 2** The on-board processor shall receive commands and data from a user-operated PC.

*Motivation:* In a spacecraft landing scenario, the lidar scanning system must interface with the spacecraft bus. The PC will take the role of the spacecraft bus in this project.

\* Assuming a 0.5m by 0.5m landing area, a 20° scan angle yields 210 independent landing sites

<sup>†</sup>The slant range is defined as the maximum range, obtained at the maximum scan angle.

**DR 2.1** The system shall receive a command from the PC to initiate operation.

- *Motivation:* The PC must be able to simulate the spacecraft bus, commanding the system to initiate operation when the hover stage is reached.
- *Verification:* A command will be sent and the operation commencement will be visually confirmed.

**DR 2.2** The system shall terminate operation upon command from the PC.

- *Motivation:* In the event of system problems, the scanning operation must be able to be terminated via the PC interface.
- *Verification:* The operator will send a terminate command to the system during a scanning operation and verify visually that operation terminates.

**DR 2.3** The system shall accept simulated Inertial Measurement Unit (IMU) data from the PC.

- *Motivation:* A real-mission implementation of this project would require knowledge of the landing craft's attitude in order to calculate a ground point's location in three-dimensional space. Landing craft motion is out of the scope of the MACULA project but the on-board software will be constructed with handles where IMU data could be easily input in the future.
- *Verification:* Known IMU data will be sent from the PC to the stationary system. The constructed map will be compared with the expected map (computed off-line based on the IMU data) in order to verify that the IMU data are being used in the analysis.

**FR 3** The on-board processor shall command the sensor package, made up of the lidar and the scanning system.

*Motivation:* Range measurements must be taken in two dimensions as per **DR 1.1**, thus the sensor package must be directed. In order to provide autonomous functionality required in a mission scenario, the sensor package must be commanded by the system's on-board processor.

**DR 3.1** The on-board processor shall store logs with timestamps of all commands sent to the lidar and actuator(s).

- *Motivation:* Command logging is critical to verifying the correct sequence of events and communications between subsystems. Logs will also be helpful in troubleshooting.
- *Verification:* Commands to various components will be issued by the on-board processor at known time intervals. The logs will be copied to the PC and commands, along with their timestamps, will be manually verified.

**DR 3.2** The on-board processor shall send actuator commands to control the orientation of the lidar beam.

- *Motivation:* Given that the system must be able to scan the terrain in two dimensions (**DR 1.1**), the reliability of the system is greatly improved if the direction of the scanning beam can be explicitly commanded. This is opposed to random motion with attitude knowledge. Explicit commanding will allow for consistent results between tests and may allow for finer scans of sub-sections of the terrain.
- *Verification:* Commands will be issued by the on-board computer and the scanning mechanism will be visually verified to actuate.

**DR 3.3** The on-board processor shall command the start and stop of lidar data collection.

- *Motivation:* In order to have user control over the state of the system, the on-board processor must be able to control the state of the lidar for starting and stopping tests.
- *Verification:* The on-board processor will be commanded by the user to turn on the lidar sensor, while not sending any commands to the motors. The user will then command the scan to stop after lidar data have been collected. The functionality of the lidar will be confirmed with command logs and stored data files.

**FR 4** The sensor package shall utilize lidar to obtain range measurements at known orientations.

*Motivation:* As per customer request, lidar is the chosen sensing method to obtain range measurements for the dynamic hazard detection and avoidance system.

**DR 4.1** The lidar shall have a minimum range of 12m or less.

- *Motivation:* In order to detect hazards, the test mock-up must have varying topography. These topographic features will be offset from the local geoid, meaning that measurements will be taken at distances less than 14.1m. This requirement allows for 2m objects, which is larger than any features that will be built and tested.

- **Verification:** The lidar sensor will be set up at known distances from a flat surface. These distances will be measured manually and be set to values at and above the minimum range of 12m. Range measurements from the lidar sensor will be compared to the manual measurements to ensure accurate measurements at a minimum range of 12m.

**DR 4.2** The lidar shall have a maximum range of 17.25m or greater.

- **Motivation:** See motivation for **DR 4.1** with the only difference being this requirement is based on slant, not nadir.
- **Verification:** The lidar sensor will be set up at known distances from a flat surface. These distances will be measured manually and be set to values below and at the maximum range of 17.25m. Range measurements from the lidar sensor will be compared to the manual measurements to ensure accurate measurements at a maximum range of 17.25m.

**DR 4.3** The lidar shall have a range error of less than 0.05m.

- **Motivation:** The scanning system should not report any hazards when scanning a flat plane. The worst-case error for this scenario would be neighboring points that have maximum error in opposite directions, such that the height between them registers as a hazard. Therefore, the range error should be less than half of the hazard height, which is approximately 0.065m as defined in Appendix C.3. With a margin of approximately 20% and rounded down to the nearest centimeter, this gives an error bound of 0.05m.
- **Verification:** The lidar sensor will be set at a known distances from a flat surface. These distances will be measured manually and be varied between the maximum and minimum range of the lidar sensor. The data output from the lidar sensor will be compared to manual measurements of the range, with no more than 0.05m difference allowed between the two measurements.

**DR 4.4** The lidar shall have a cross range error of less than 0.05m. (See Appendix A for a definition of cross range error.)

- **Motivation:** As per **DR 1.4**, any two consecutive data points collected by the lidar system will be separated by a distance of at most 0.1m. If the maximum cross range error is assumed, then the error must be less than 0.05m such that in the worst case scenario, separate measurement data points will not overlap.
- **Verification:** The specifications of any lidar range measurement device used will be reviewed to determine that the maximum cross range error requirements are met. Additionally, the lidar obtained will be tested at a range of 15m and data output will be analyzed to verify that range measurements returned are  $15 \pm 0.05m$  (as defined in **DR 4.3**).

**DR 4.5** Worst-case return signal angular uncertainty\* shall be less than or equal to 0.15°.

- **Motivation:** Motivation for this design requirement is given in Appendix A
- **Verification:** Error will be determined from manual measurements of the beam optics through the use of an optical bench.

**DR 4.6** Lidar range and beam attitude measurements shall be taken within one microsecond.

- **Motivation:** To construct any meaningful point cloud in a dynamical system, measurements that relate to one another, such as range and attitude, must be taken as close to the same time as possible to reduce the error from measurement latency. The one micro second time is derived by making the assumption that the beam is hitting a rotating mirror or prism. The error is then  $360^\circ \times 40\text{Hz} \times \text{measurement latency} = 0.015^\circ$ . 40 Hz will be higher than the rotation rate of any mirror or prism in the system and 0.015° is 10% of the attitude error from **DR 4.5**. The measurement latency time is then 1.042  $\mu s$ , rounding down to 1  $\mu s$ . If the rotation is at a known rate then the error can be reduced depending on the accuracy of the timing and the encoder by taking the time between measurements and multiplying it by the rate and subtracting it from the measured angle. However doing this may take two quadrature decoders for each encoder, one to measure position and the other to measure rate.

---

\*The worst-case return signal angular uncertainty is defined as the sum of uncertainty due to angular position uncertainty, beam diameter (spot size), and beam divergence. Beam divergence and beam spot size both create angular uncertainty in where the return is measured from.

- **Verification:** A pin on a micro-controller can be set immediately before the measurements take place and then cleared once they finish. The resulting square wave can then be seen and measured on an oscilloscope.

**FR 5** The sensor package shall transmit data to an on-board processor or DAQ.

*Motivation:* Raw data outputted by the sensor package must be compiled and saved in usable formats for use in further analysis.

**DR 5.1** The lidar shall send range data to the on-board processor or DAQ.

- *Motivation:* The measurement data outputted from the lidar sensor must be collected, conditioned, and stored such that it is usable by the on-board computer or DAQ for further processing. Simple lidar sensors only output data, and do not store this data themselves. This data must be sent to an external source for compilation and storage.
- **Verification:** The lidar sensor will be connected to an on-board computer or DAQ and will be positioned in front of a flat surface. The sensor will then be commanded to take stationary range measurements of the flat surface, with measuring only one point on the surface. Data being outputted directly by the lidar sensor as well as captured data outputted from the on-board computer or DAQ will be compared to ensure proper transmission of data through the electrical interface.

**DR 5.2** The beam attitude measurement shall be sent to the on-board processor or DAQ.

- *Motivation:* Beam attitude data must be collected, conditioned, and stored along with the lidar range data in order to properly represent a point in three dimensional space. This data must be combined with the lidar range measurements during analysis. This data must be sent from the attitude measurement devices to the on-board computer or DAQ.
- **Verification:** The attitude measurement devices will be set up along with the scanning system. Attitude measurements will then be taken from the devices and recorded by both an external computer connected directly to the devices and the on-board computer or DAQ. The data outputted by the devices and the data outputted from the on-board computer or DAQ will be compared to ensure proper transmission of data through the electrical interface.

**FR 6** The on board processor shall translate the range and attitude data into a three-dimensional point cloud.

*Motivation:* Analysis of the terrain will be performed on a topographic map, requiring a change of coordinate system from range and attitude.

**DR 6.1** Range and attitude data shall be transformed into  $(x,y,z)$  coordinates.

- *Motivation:* The measured range and pointing attitude data must be formatted or transformed in a way that can be analyzed for hazards. Transforming into three-dimensional Cartesian coordinates creates a point cloud that represents the ground terrain as seen from the viewpoint of the lidar. Such a map can be verified by measuring the real-world geometry being scanned. The need to verify the accuracy of the scan drives the requirement to have models that can be compared directly.
- **Verification:** After range data are measured from the lidar and attitude data are taken from the scanning system, the transformed points will be compared for accuracy against measurements made on the physical mock-up. From this comparison, the uncertainty in the measurements can be characterized.

**DR 6.2** Uncertainties in range and attitude shall be propagated into uncertainty in  $(x,y,z)$  coordinates.

- *Motivation:* A model of the uncertainty in the system is critical for knowing the confidence that the algorithm has when identifying hazards and topographic features. Tests of specific components can isolate this uncertainty and may help to improve the overall accuracy of the system.
- **Verification:** Points measured in the physical test bed can be compared against ideal scan data (assuming no error or uncertainty in any components). This comparison can be done at points spanning the map and can be done across many test scenarios to validate and characterize the uncertainty models.

**FR 7** The on-board processor shall analyze the 3D point cloud for hazards.

*Motivation:* Hazards must be identified in order to select a touchdown zone that does not violate the landing requirements for the mission.

**DR 7.1** Hazardous areas shall be identified if the area contains a hazard with height defined in section C.3 of the appendix, or if touchdown in the selected area would place the lander base more than 15° off of vertical.

- *Motivation:* The landing craft must be able to land in a zone that is deemed safe. In order to deem a zone safe, the on-board software must be able to identify hazards based on sizes and shapes that would exceed the allowable landing requirements.
- *Verification:* Hazardous objects and terrain will be deliberately placed during testing so that the on-board detection system can be tested for accuracy and consistency. The geometry and location of these hazards will be known to an accuracy better than the calculated system accuracy, making these hazard detections directly verifiable.

**FR 8** The on-board processor shall select an acceptable landing site.

*Motivation:* Landing of spacecraft on foreign space bodies provides significant risk to both the spacecraft and its mission objectives. As such, the ultimate purpose of a dynamic scanning system for spacecraft landing is to choose acceptable landing locations from a scanned area that will not jeopardize the mission. In addition to the detection of hazards, the scanning system must have the ability to identify areas of terrain within the landing requirements of the mission.

**DR 8.1** The selected landing site shall be a square measuring 0.5m by 0.5m when projected onto the plane of the ground.

- *Motivation:* The selected landing zone must be able to fully contain the footprint of the lander.
- *Verification:* A physical mock-up scene will be constructed with geometry known to an accuracy better than the accuracy of the lidar scanning system. The selected landing site will be confirmed based on the physical model.

**DR 8.2** The landing site selected as “safe” (defined in App C.3) shall not contain any terrain or obstacles that exceed the landing safety requirements of the mission.

- *Motivation:* The lander must be able to land in a zone deemed “safe” by the algorithm. This requires that landing at that site would not place the lander in an orientation that does not comply with the mission requirements (**DR 7.1**).
- *Verification:* A mock-up landing area containing multiple suitable landing sites will be constructed. Construction of this map may be assisted by software prior to passing the data into the hazard detection and landing site algorithm.

**DR 8.3** In the event that no suitable landing site is found, the acceptable threshold for safety will be lowered until one appears.

- *Motivation:* In order to serve the intended function of the system, the landing craft must be instructed to land in a specific location after scanning the terrain below it. Since the project aims at landing on previously unmapped terrain it may be the case that there are no acceptable landing sites within the field of view of the sensor. In this case, the craft must be instructed to land in a zone that complies with the requirements as closely as possible.
- *Verification:* A mock-up landing area known to contain no suitable landing zones will be constructed. Construction of this map may be assisted by software prior to passing the data into the hazard detection and landing site selection algorithm. The on-board software must then be able to select the landing site by iteratively loosening the landing requirements until at least one zone is deemed suitable.

**FR 9** The system shall generate output readable by the PC.

*Motivation:* Results of the scan and analysis are only useful if they are provided as output to direct the lander in a mission scenario. In the proof-of-concept scheme the PC serves the role of spacecraft flight computer.

**DR 9.1** The system shall generate health and status information readable by the PC in real time.

- *Motivation:* Knowing the state of the system at different times during the mapping operation is important for troubleshooting and for overall system validation. Generating this information is also important for subsystem communication on a landing craft that would house future iterations of this product.

- Verification: The system will be commanded to known states and tested with failure cases at known timestamps so that health and status logging data will have expected content that can be manually verified. Simulated system problems will be inserted into the health and status information and this will be read in real-time by the operator on the PC.

**DR 9.2** Range measurements from the lidar and attitude measurements from the pointing system shall be readable by the PC.

- *Motivation*: The raw range and attitude information must be stored either on the on-board memory or on the PC so that the measurements can be compared against measurements of the physical test bed.
- Verification: Test range and attitude data objects will be both logged on the on-board processor and sent to the PC. The PC will read and display the data, which can then be manually checked against the logged data for correctness.

**DR 9.3** The three-dimensional point cloud shall be readable by the PC.

- *Motivation*: Storing the point cloud information is important for visually confirming the output of the on-board sensors and translational math when placing the points in three-dimensional space. The point cloud can also be used for direct comparison of scanning system measurements to measurements of the physical test bed.
- Verification: Three-dimensional point cloud data objects will be both logged on the on-board processor and sent to the PC. The PC will read and display the data, which can then be manually checked against the logged data for correctness.

**DR 9.4** Identified hazard locations shall be readable by the PC.

- *Motivation*: The output of the hazard detection algorithm must be directly verifiable with measurements of the physical test mock-up
- Verification: Hazard location data objects will be both logged on the on-board processor and sent to the PC. The PC will read and display the data, which can then be manually checked against the logged data for correctness.

**DR 9.5** The selected landing location shall be readable by the PC.

- *Motivation*: The output of the landing site selection algorithm must be directly verifiable with measurements of the physical test mock-up. This is analogous to sending the output of the scanning system to the spacecraft bus with identification of a safe landing zone.
- Verification: Landing location data objects will be both logged on the on-board processor and sent to the PC. The PC will read and display the data, which can then be manually checked against the logged data for correctness.

### 3 Key Design Options Considered

The success of the MACULA project hinges on the solutions to a few key challenges that have very diverse solution spaces. With applications of lidar so varied, it is important to explore these spaces for solutions that others have created for similar problems, and then to adapt, improve, and integrate them to best suit the needs of the MACULA project.

The first design trade is for the lidar hardware itself. This explores the commercially available options for a lidar (or multiple) that could be used to map terrain. Selecting a lidar suitable for the needs of the MACULA project will be a driving factor in the ability to produce an accurate topographic map, and therefore a driving factor in all levels of project success.

The second design trade is for a scanning mechanism, which is essentially a subset of the first trade. This trade explores the design options for a beam-steering mechanism, which, along with the lidar selection, will be critical for being able to produce accurate maps.

Lastly, a design trade is performed on the hazard detection algorithm. This design choice is important to higher-level success of the project, where on-board software must be able to identify landing hazards and select a suitable landing zone. This trade explores mathematical solutions to this problem, with importance placed on what implications certain algorithms could have on the scanning pattern, and vice versa.

These three components of the project are necessary for baseline design and will have far-reaching effects for the remainder of the project. The following subsections will describe the design options in detail, and the following section will present the associated trade studies.

#### 3.1 Lidar Sensor

Lidar, which is an abbreviation for Light Detection and Ranging, is a technology that evolved from radar (Radio Detection and Ranging) beginning in the 1960s. Radar uses the deflection of radio waves to detect objects, whereas lidar uses the deflection of laser beams typically in the visible to near-infrared regions of the electromagnetic spectrum. The advantage of lidar over radar is the high directionality of the laser measuring beam, which can be used to detect the distance to an object at very specific locations. Measurements are typically made by measuring the time that a beam of light takes to reach a surface, reflect, and arrive back at the lidar's location. Another method is to measure the phase difference of the reflected light to the source light, and to modulate the wave such that the returning information is unique to a particular distance<sup>16</sup>.

Lidar as a technology has many applications. It has been used on the ground for proximity sensing, on airborne systems for mapping of topography, forests, and glaciers, and on spaceborne systems for altimetry<sup>16</sup>. Lidar is used in a wide variety of active research areas as well, such as the study of clouds and atmospheric water composition<sup>5</sup>.

For this wide array of applications, lidars have diversified greatly since the first applications of laser range measurements in the 1960s. Several of these lidar groups have potential applications for the MACULA project: fixed-beam lidar, scanning lidar, optically-segmented lidar, and flash lidar. These systems can be purchased commercially as integrated units or constructed from a lidar and scanning system components. These various lidar classifications are discussed further in the following subsections.

##### 3.1.1 Building a Lidar

The first option to fill the lidar sensor requirement of the MACULA system is to build a lidar sensor. This would require the purchase of a laser emitter in the visible to near-infrared range, as well as a detector of the same frequency. In addition, this would require the construction of hardware and software that would provide precise timing synchronization between the emitter and detector, as time is the measurement by which lidar sensors are able to calculate range.

The advantage to purchasing individual components is that the selection and implementation of each component can be fine-tuned to fit the requirements of the MACULA system. Each component can be individually considered to produce the accuracy and range necessary to fulfill **FR 4**. Additionally, with each component purchased separately, the cost of each component can be weighed with its necessary performance, which allows for the project budget to be used more efficiently.

A disadvantage to building a lidar sensor is the added complexity that results from the precise timing requirement of the sensor. A timing error of only  $1ns$  would result in a range error of  $0.3m$  according to the speed of light propagation, which is well over the minimum range accuracy of the MACULA system, as defined by **DR 4.3**. As

such, a large amount of time and effort would be necessary to ensure proper time synchronization. This added effort would be beyond the scope of the MACULA project, and would detract from other desired results of the system, so ultimately this option will not be considered in the trade study.

Table 3: Advantages and Disadvantages of Building Lidar

Advantages	Disadvantages
Highly customizable	Hardware Complexity
More Control Over Cost	Added Scope to Project

### 3.1.2 Fixed-Beam Lidar

The first category of commercially available lidar sensors to consider is single, fixed-beam lidar. These devices are the simplest form of lidar, with the sensors emitting and detecting a single laser pulse to achieve a range measurement in a single direction. Use of such a sensor in a scanning system would require mechanical redirection of the beam to move the pointing direction over a two dimensional scan surface. The advantage to this is that it opens a new solution space of all the methods that could be used to redirect the lidar beam to form a scan pattern, which allows direct control over **DR 4.5**. Fixed-beam lidars can be found for prices ranging from hundreds of dollars to thousands of dollars<sup>10</sup>, depending on their accuracy and range capabilities. This variation of cost also means that fixed-beam lidars can be found with a wide variety of maximum ranges, which means that a sensor with qualities more tuned to the MACULA system can be selected, which allows more control over **DR 4.2**.

A disadvantage to using a single-beam lidar would be the added mechanical complexity from the scanning system. Using a fixed-beam lidar would require that either the beam or the entire lidar sensor be redirected over a predetermined pattern. The mechanical system would also result in uncertainties in pointing accuracy that would have to be characterized and accounted for in software, which works against **DR 4.5**.

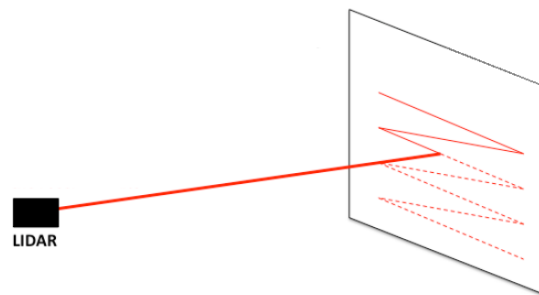


Figure 3: Conceptual diagram of single-beam lidar used for scanning a surface.<sup>4</sup>

Table 4: Advantages and Disadvantages of Fixed-Beam Lidar

Advantages	Disadvantages
Versatility	Mechanical Complexity
Low Cost	Complex Error Propagation
Wide Variety of Range Distances	

### 3.1.3 Multiple Fixed-Beam Lidars

An alternative to using a single fixed-beam lidar would be to use multiple fixed-beam lidars. In terms of the scanning mechanism, this would be the same as using a single fixed-beam lidar, except the beam of each lidar would be redirected individually by separate mechanisms. Using multiple sensors would decrease the degree of mechanical actuation for each sensors, thus decreasing the necessary range of motion for the scanning system actuators. Additionally, the total time to scan the terrain at the same resolution would be reduced by a factor of the number of lidar sensors used, which benefits **DR 1.5**.

A disadvantage to using multiple lidar sensors is the added mechanical and software complexity. If the lidars are mounted on separate actuators, this requires independent actuation systems, each with their own controls and uncertainties that would have to be characterized. The lidars could also be mounted to the same actuation system, but at different angles such that the actuator(s) would only need to move over a portion of the full range in order to achieve the full scan. Either scenario would add complexity to the DAQ system and to the requirements of the hazard detection algorithm, as defined by **DR 7.1**, since the algorithm would have to account for points coming in simultaneously at different locations on the terrain. A beam emitted from one lidar could also be received by another, which could introduce significant errors to the map and prevent the MACULA system from meeting the accuracy requirements under **FR 4**. Lastly, added lidars means added cost for a project element that is likely to take up a significant portion of the project budget to begin with.

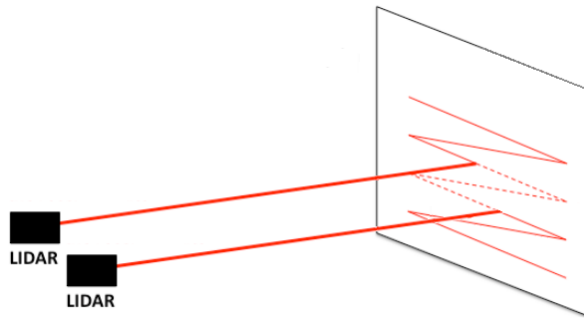


**Figure 4:** Conceptual diagram of multiple single-beam lidars used for scanning a surface.<sup>4</sup>

Table 5: Advantages and Disadvantages of Multiple Fixed-Beam lidars

Advantages	Disadvantages
Less Mechanical Actuation Per Sensor	Mechanical Complexity
Reduced Scan Time	Sensor Interference
	High Cost

### 3.1.4 Scanning Lidar

Another option for the lidar sensor would be to use a sensor with integrated scanning capabilities, where the off-the-shelf sensor already provides the ability to scan along one or two dimensions. The most common motion of a sensor of this type is a circular rotation about its vertical axis, as seen in Fig. 5. This type of sensor is most commonly used for autonomous automobile and robotic applications, where a 360° range scan is necessary for full characterization of the surrounding environment<sup>12</sup>. Using this type of sensor for MACULA’s application would simplify the mechanical design of the system, as the sensor would not need to be actuated as long as the built-in scan coverage reaches at least 20° off of nadir in both directions.

A disadvantage to using a scanning lidar would be added cost to the project. These sensors generally cost significantly more than fixed-beam lidars. Additionally, both the scan speed and angular resolution are fixed properties of the system and will not necessarily fit the needs of the MACULA system, which works against **DR 4.5** and **DR 1.4**.

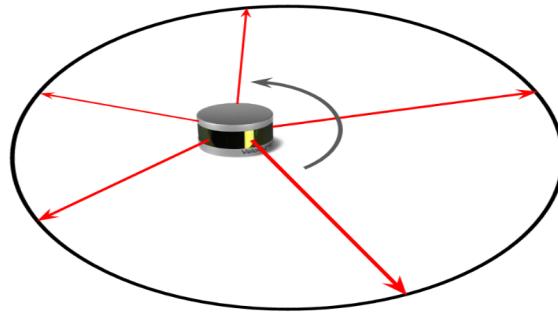


**Figure 5:** Conceptual diagram of Velodyne Puck LITE LiDAR scanning its environment<sup>12</sup>

Table 6: Advantages and Disadvantages of Scanning Lidar

Advantages	Disadvantages
Mechanical Simplicity	High Cost
Quick Actuation	Fixed Angular Resolution

### 3.1.5 Optically Segmented Lidar

Another possibility for the lidar sensor is to use optically segmented lidars, where the laser beam is run through an optical filter that fans the beam over a specified angle range. This system provides the ability to scan a larger region with a single pulse, where an array of points are scanned along one dimension. This system would reduce the amount of actuation needed for the full scan, providing an increased scan speed to meet **DR 1.5** and decreased mechanical complexity of the scanning system. Additionally, these sensors can be found in modular configurations, where the sensor can be modified by various optical filters to fill a variety of resolution requirements described by **DR 1.4**.

A disadvantage to segmented lidars is that they generally have low angular accuracy, which greatly increases the accuracy constraints on the constructed mechanical actuation system and works against **DR 4.5**. Furthermore, the resolution of these sensors is fixed by the optics being used, which decreases the flexibility of the system for different mission requirements, and may not allow MACULA to meet **DR 1.4**.

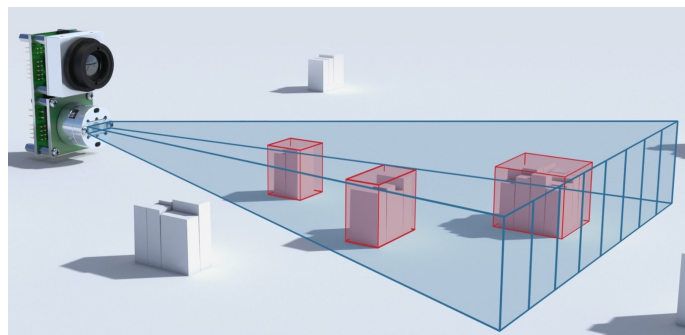


**Figure 6:** Conceptual diagram of LedderVu, an optically segmented lidar sensor.<sup>9</sup>

Table 7: Advantages and Disadvantages of Optically Segmented Lidar

Advantages	Disadvantages
Larger Scan Region for Single Pulse	Low Accuracy
Mechanical Simplicity	Static Resolution
Customizable	

### 3.1.6 Flash Lidar

The final option considered for the lidar sensor is a flash lidar. These sensors diffuse a single laser beam over the entire field of view. The detector can then obtain the range measurements simultaneously for each of the "pixels" on the map<sup>18</sup>. This type of sensor differs from optically segmented lidar in that flash lidar detectors capture a large amount of data points using individual pixels (analogous to a camera), while an optically segmented lidar only uses a small number of segments. These sensors provide the ability to scan a very large region with a single pulse. This simplifies the mechanical design of the system, as flash lidar would require no mechanical actuation as long as the sensor's field of view extended to more than 20° off of nadir. Additionally, with many range points being measured simultaneously, the overall time of scan is significantly reduced, which would meet **DR 1.5**.

The major disadvantage to flash lidar is the cost, with lower-end flash lidars being in the range of \$50,000. This extremely high cost immediately disqualifies flash lidar for use in the MACULA system. Another disadvantage is the fixed scan resolution of flash lidar, which limits the versatility of the system unless the sensor is actuated. This limits the fulfillment of **DR 1.4**.

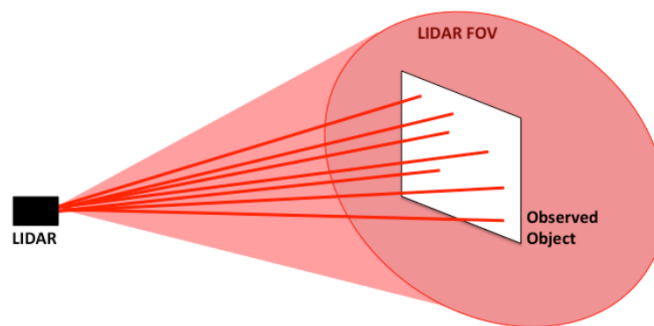


Figure 7: Conceptual diagram of flash lidar used for scanning a surface.<sup>4</sup>

Table 8: Advantages and Disadvantages of Flash Lidar

Advantages	Disadvantages
Scan Region	Very High Cost
Mechanical Simplicity	Fixed Static Resolution
Small Scan Time	

## 3.2 Scanning Mechanism

One of the most fundamental requirements for this system is the ability to scan. In order to meet both **DR 1.1** and **DR 1.2**, a scanning system is required. This requirement opens up many design options to consider. In the following, these options will be presented along with their advantages and disadvantages within the scope of the project. It is important to note that these scanning systems are most applicable to a system with a fixed-beam lidar, but would also need to be applied to optically segmented lidar (to increase scan resolution) or scanning lidar (to increase the dimensionality/resolution of the scan).

### 3.2.1 Mechanical System

A mechanical system for steering the lidar, such as the one shown in Fig. 8 below, is a common solution in the industry to this problem. Gimbals, for example, are commonly used to mount cameras to drones in order to focus the camera on specific targets while the drone is moving. This mechanical system would require at least two motors in order to actuate the pitch and lateral motion of the lidar system to accomplish **DR 1.1** and **DR 1.2**.

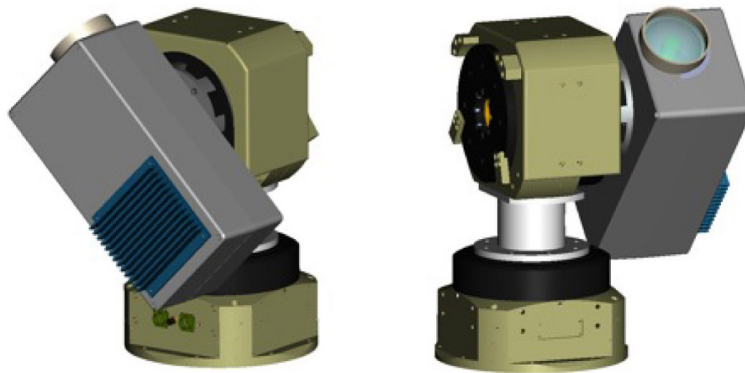


**Figure 8:** Mechanical system used to actuate a lidar system.<sup>19</sup>

A large advantage of mechanical systems is that the pointing accuracy is primarily limited by the angular accuracy of the actuator(s) and/or encoder(s) used for steering of the lidar. Commercially available encoders are readily capable of meeting **DR 4.4**. Mechanical systems are also well established in many industries for actuating and controlling components, meaning that the design reference base is large and the TRL is not an issue. Lastly, a mechanical system would be able to apply any desired scanning pattern, including finer secondary scans of potential landing zones.

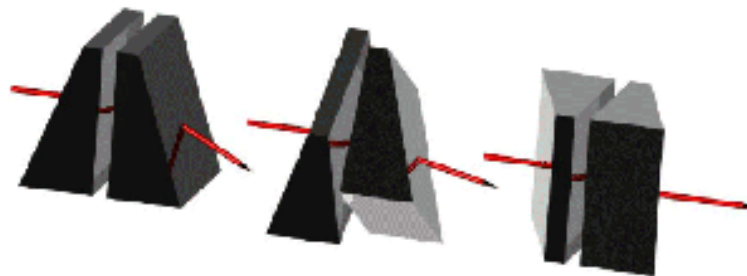
A major disadvantage of a mechanical system approach is the time to scan. This is due to a mechanical system having a high mass and moment of inertia. Physically rotating the lidar body for every scan point requires a heavy and robust mechanical system that will likely experience overshoot when changing the direction of movement. One way to mitigate this problem is to conduct the scan slower, but this hampers the ability of the system to meet **DR 1.5**. Another disadvantage of a mechanical system is that physical translation of the lidar sensor is unavoidable. Appendix B defines and mathematically explores this added source of error. Any misalignment of the lidar to the mounting frame must be characterized and either propagated as error or accounted for in software.

Table 9: Advantages and Disadvantages of Mechanical System

Advantages	Disadvantages
Actuation Complexity for Desired Scan Pattern - A mechanical system could easily implement any scan pattern chosen	Cost - The cost to build the entire mechanical system would be between \$1500-\$2000.
TRL - Mechanical systems have been used and tested in real world scenarios	Moment of Inertia of Rotating Components - Due to the large size of the mechanical system needed to move the lidar, the moment of inertia would be quite large
	Hardware Design Complexity - Mounting the lidar to the mechanical system and ensuring that it was mounted accurately would be quite involved and complex

### 3.2.2 Risley Prisms

Another method of achieving beam steering is through the use of Risley Prisms. A Risley Prism scanning system consists of two circular wedge prisms mounted in series. Risley Prisms are based off the principle that light bends when passing through a translucent or transparent object at an angle. This phenomenon can be characterized according to Snell's Law. Risley Prisms take advantage of this behavior by refracting light twice in a controlled manner. By rotating each prism separately, a beam passing through the prism system can be steered in two dimensions<sup>15</sup>, limited by the maximum beam deviation for the two-prism combination<sup>13</sup>. Therefore if 10 degree beam deviation prisms were used, design requirements **DR 1.1** and **DR 1.2** would be satisfied. An illustration is displayed below in Fig. 9. Using a Risley Prism scanning system would still require obtaining a highly accurate motor system for actuating the prisms.



**Figure 9:** Diagram of Risley Prism functionality. On the far left, prisms are orientated for maximum beam deviation. On the far right, prisms are orientated such that there is no deviation. Image obtained from OPTRA, Inc.<sup>15</sup>

Use of a Risley Prism scanning system poses several important advantages for the project overall. Firstly, scanning with a Risley Prism system would likely take the least amount of time in comparison to the other scanning system options considered. This would be advantageous for completing design requirement **DR 1.5**. The reason for this is that Risley Prisms have small moments of inertia and are relatively insensitive to vibration<sup>11</sup>. The motion required for beam redirection is small compared to a mechanical system, so the scan can be completed significantly faster. Another advantage of the Risley Prisms is their low pointing error, meaning that the accuracy of the scan would be primarily limited by the accuracy of the motors and/or encoders used to rotate the prisms. This advantage relates directly to **DR 4.5**.

Risley Prisms can also be purchased with coatings that improve the refractive properties for specific wavelengths<sup>13</sup>. This means that prisms could be purchased to match the specifications for any chosen lidar. The final advantage associated with Risley Prisms is with their hardware simplicity. This is due to the fact that Risley prisms will not require a

slip ring. Slip rings or wireless communication could be used to transfer information from and to a rotating component, but removing the need for this interface would simplify the design from a mechanical and software standpoint.

Although Risley Prisms offer many advantages over other systems, they also present several foreseeable problems. A notable issue is that Risley Prisms are an active area of research, and are not well established in the industry for the applications in the MACULA project. Risley Prisms are also optically challenging, including potential issues with alignment, internal reflections and losses, amplified beam divergence, and issues with the lidar receiver field of view. Although there are a large number of potential optical issues, it should be noted that the team has access to help from graduate students in Professor Thayer’s Active Remote Sensing Lab (ARSENL). This could prove to be an invaluable resource for help on optics.

Risley Prisms also pose some potential problems aside from the optical challenges listed above. Firstly, the scan shape generated using Risley prisms is more complex than what the alternative scanning systems are likely to produce. This would be a complication in achieving design requirement **DR 3.2**. Rather than a grid pattern or concentric circles, the Risley Prisms would produce either a spiral pattern if spun in co-rotating directions, and a rosebud pattern if spun in counter-rotating directions<sup>13</sup>.

Using a Risley Prism scanning system provides some distinct advantages to the other systems listed, but also poses risks due to being a less-established method in the industry that is likely to pose optical and software challenges to the team.

Table 10: Advantages and Disadvantages of Risley Prisms

Advantages	Disadvantages
Error - Error solely due to motors. In the pitch direction, Risley Prisms improve on the uncertainty in the motors.	Scan Complexity - Rotation of the prisms in opposite directions results in a complicated scan pattern. A grid scan cannot be accomplished.
Time to Scan - Risley Prisms have a small moment of inertia and can be moved quickly with precision.	TRL - Risley Prisms are an active area of research. They are an advanced optical technology, and the team has essentially no optical experience.
Hardware Design Complexity - Prisms are rotated independently so there is no need for a slip ring. Mounting and connecting to motors is not anticipated to be difficult.	
Cost - Circular Wedge Prisms generally cost below \$100. Motors will not need to be as powerful.	

### 3.2.3 Optical Mirrors

Actuated optical mirrors are a common method to achieve accurate beam steering with laser systems within various industries. Actuated optical systems are based on the law of reflectivity, which states that the angle between the beam and the reflective surface (called the angle of incidence) is equivalent to the angle between the surface and the reflected beam (called the angle of reflection), as seen<sup>11</sup> in Fig. 10. Using this principle, optical mirror scanning systems such as the one seen in Fig. 11 operate by rotating the mirrors about multiple axes to steer the beam in two dimensions, thus satisfying requirements **DR 1.1** and **DR 1.2**.

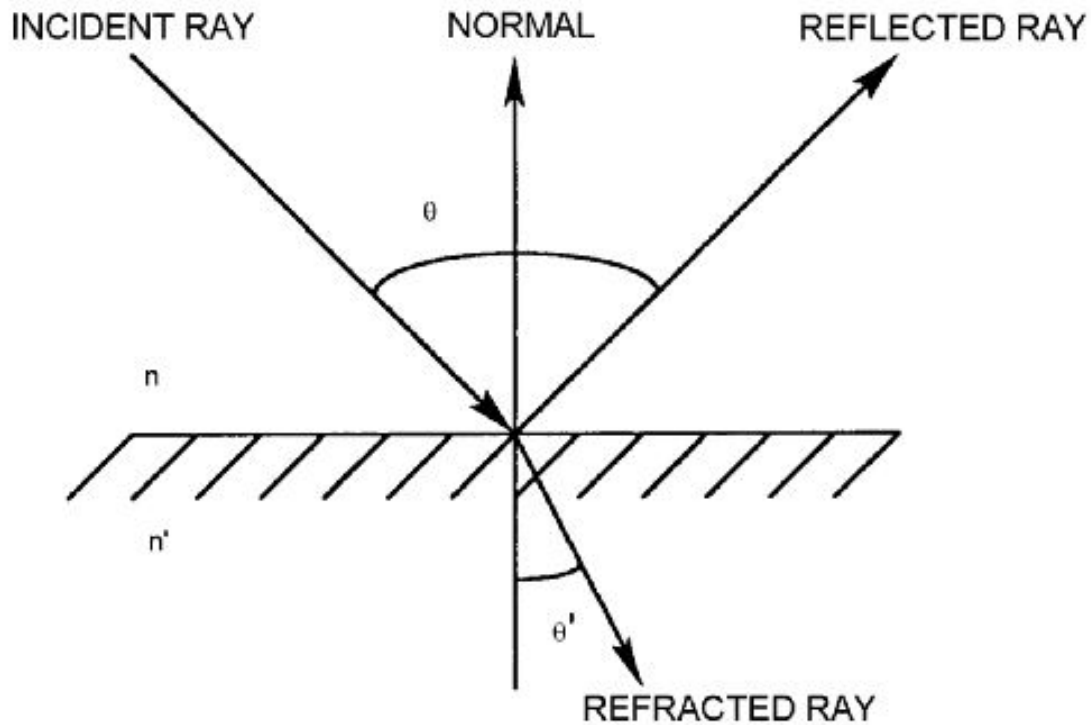


Figure 10: The Law of Reflection

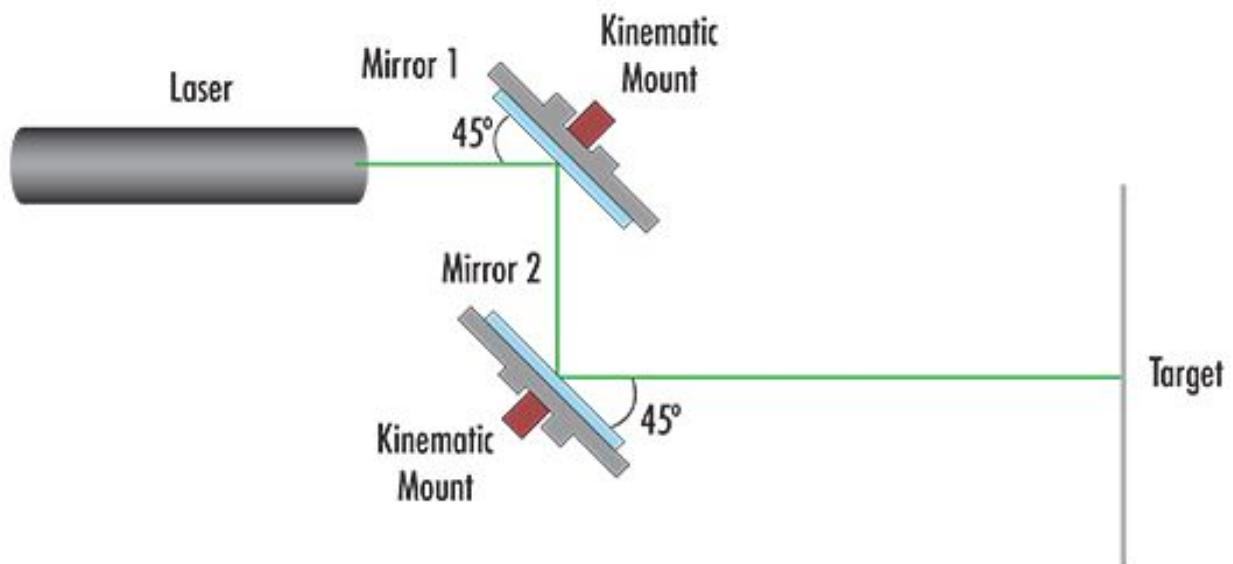


Figure 11: A basic mirror configuration

There are many advantages to using an actuated optical mirror system on this project. Optical mirrors are simple to utilize due to the law of reflectivity and flat mirrors introduce no additional uncertainty due to beam divergence, and angular uncertainty only due to imperfections in the flatness of the mirror, helping to satisfy requirement **DR 4.5**<sup>3</sup>. The high-quality mirrors offered by companies are rated for various beam frequencies, creating versatility with the design options in the lidar system. Prices on these mirrors vary widely, from tens to thousands of dollars, thus creating

a diverse market from which to choose a optimal system within the budget of the project. Due to the simplicity from the law of reflectivity, an optical mirror configuration can be designed for a plethora of scan patterns over a two-dimensional space<sup>11</sup>. The speed at which this pattern is completed is limited only by the speed at which the actuators can accurately move the mirrors without inducing large vibrations, helping to meet requirement **DR 1.5**. Integration within the system as a whole would prove simple since the mirrors would be rigidly mounted to the motors, though this may require slip rings.

However, while optical mirror systems have many advantages, there is the potential for significant error through the law of reflectivity. As previously stated, the angle of incidence is equal to the angle of reflection, and due to this any error in the optical alignment of the mirrors is doubled<sup>11</sup>. It can then be further implied that this error has the potential to grow exponentially for a multi-mirrored system by the following worst-case equation:

$$E_{tot} = 2^n \sum_{i=1}^n (E(i)).$$

This potential for error restricts the capabilities of the optical mirrors to satisfy requirement **DR 4.4**.

Table 11: Advantages and Disadvantages of Optical Mirrors

Advantages	Disadvantages
Technologically ready: Actuated optical mirrors have been utilized throughout industry.	Error: The angle error is doubled by law of reflectivity.
Pattern diversity: Beam steering is easily achieved and allows for a variety of patterns.	
Time to scan: Small moments of inertia for each mirror allows for easy actuation and faster scan times.	
Cost: There is a diverse selection of mirrors at affordable price ranges, \$10-\$1000, with the manufacturing quality needed.	

Optical mirror systems are limited by the uncertainty in their measurements. However, if proper care is taken in mounting and configuration design, their advantages could prove valuable to this project.

### 3.2.4 Translational Mechanical Scanning System

Another mechanical scanning system considered is one in which the lidar is moved in a purely translational manner. This system would consist of a large scanning track on which the lidar would move in two directions. A diagram of such a system is shown below in Fig. 12. This option was quickly ruled out by the team and was not considered in the scanning system trade study. This is due to the fact that the scanning system would have to have the same footprint size as the area being scanned, and moving over this area translationally is prohibitively slow for the purpose of this project.

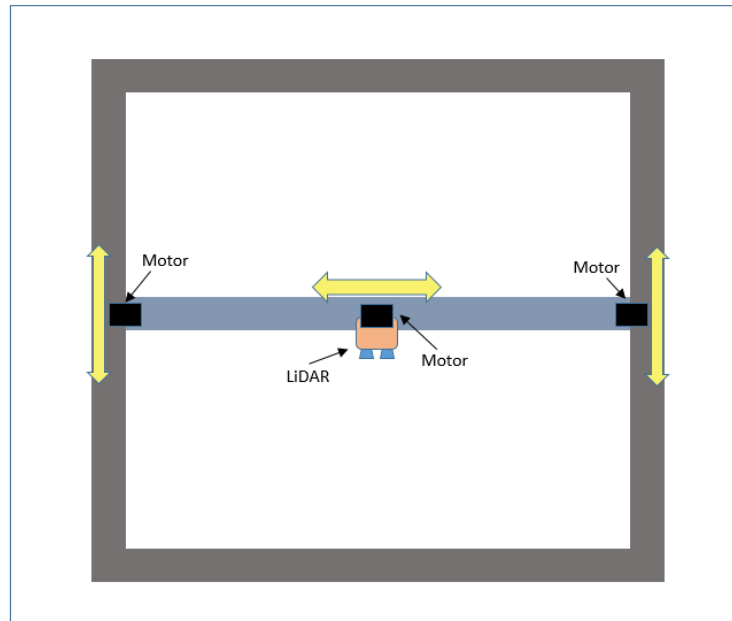


**Figure 12:** Example of a translational based scanning system.

Although this design was deemed unsuitable for the project, it does have several notable advantages. For instance, the scanning accuracy of a system such as this would be much better than the other options. When using a completely translational system, the only angular uncertainty in the system is due to the lidar mount and the frame for translational movement. Angular uncertainty is particularly important to mitigate since it causes the uncertainty in the final measurement to grow approximately linearly with distance. Additionally, the scan pattern is very simple to design for this system since the lidar could be moved to point at any point within the scan area. The technology readiness of this system would also be an advantage as similar systems have been developed many times before.

However, the disadvantages significantly outweigh the advantages of this system for the MACULA project. Firstly, achieving both the scan time and spatial resolution requirements with this system would be next to impossible. With a purely translational system, the lidar would need to physically move over the entire potential landing zone. Due to the size of the potential landing zone, achieving a highly resolved scan by this method would require rapid movement. The electrical and mechanical complexity of this system would also be a downside. Moving electrical components over such a large area would be a challenge. In addition, the sheer size of the scanning apparatus for this method would be challenging and expensive to construct. All in all the large size and lack of feasibility for this design quickly ruled it out.

Table 12: Advantages and Disadvantages of Translational Mechanical Scanning System

Advantages	Disadvantages
Error - Error solely due to precision with which the motors can be moved. No angular uncertainty.	Time to Scan - Likely impossible to cover entire possible landing zone in 60 seconds.
Scan Complexity - System could easily be told to move to any point in landing zone with a simple command to two sets of motors.	Hardware Design Complexity - Size of system would be a challenge along with numerous moving electrical components.
TRL - Similar systems have been built, tested, and used before.	Cost - Same cost of motors along with a large cost for materials.

### 3.3 Hazard Detection Algorithm

In order to direct the lander to a suitable landing site, a hazard map must be constructed to identify obstacles and unsuitably rough terrain. As per **FR 6** this map will be constructed by passing the range and attitude data to the on-board processor, which will then construct a topographic map that must be analyzed for hazards. The construction of this map from data will not be considered in the algorithm trade because the methods for such a process are well established and there are no high-level trade options for completing the task as it amounts to a coordinate transformation. Additionally, once a hazard map has been constructed the landing site may be selected by implementing the Stroking Neighbor Method, described in Appendix D, which is guaranteed to find a solution and simple to implement. The hazard detection algorithm required by **FR 7** will be the novel part of the system software package, so the software trade will investigate conceptual design options for application-specific hazard detection methods.

The most basic hazard detection algorithm that can be applied to this scenario is the Simple Filter. This filter looks at the height value of each measured point relative to the nadir ground level, and marks the point as safe or hazardous based on that height value alone. This algorithm is capable of detecting basic hazards on an otherwise flat ground, but will provide poor results in many scenarios. It is included as a baseline algorithm to ensure that the criteria and weights in the trade study are selected properly.

Most of the algorithms applicable to this scenario can be divided into two categories. The first applies smoothing techniques to the point cloud to approximate the ground surface, making the protrusion of obstacles and areas of particularly rough terrain easier to identify. The second technique is to look at the gradient of the height values over the map. Areas of sharp height change can be identified as hazards, and areas of steady slope can be marked as hazardous if the slope is above the mission requirements or the lander's ability.

One challenge that applies to all scenarios is that the distribution of points on the ground will be made non-uniform by any irregularities. Areas will be more dense or more sparse depending on obstacles and the angle of the terrain relative to the scan angle from the lidar. The name "shadowing" is given to the phenomenon of areas of the map being unscannable due to obstacles and terrain. This is explained in more detail in Appendix C.1.

#### 3.3.1 Smoothing Techniques

The first technique that can be used to detect hazards involves constructing a low order approximation to the surface that intentionally aliases protruding features, then subtracting that surface from an un-aliased map. The difference between these two will be small where the terrain is relatively smooth and large where there are obstacles. One important drawback to this methodology is that interpolatory approximations lose robustness as the domain they are attempting to approximate shrinks, and also that adding points to the domain changes the entire structure of the approximation. This makes these methods ill-suited to working with serial data input. Even if the map were to be processed in multiple patches the accuracy may be compromised significantly due to effects like the Runge Phenomenon where points spaced in certain ways cause the approximation to differ dramatically from the surface it is attempting to approximate. There are two ways to construct a low order map: nodally and modally. These methods are described below.

##### 3.3.1.1 Nodal Surface Approximation

Nodal approximation methods are in essence direct interpolation methods. The simplest such method is Lagrange interpolating polynomials. These polynomials are constructed to exactly interpolate at the given points and be zero at all other points so that their sum exactly recreates the known points and approximates the surface elsewhere. In these methods the polynomial degree is dictated by the number of points to which the surface interpolates.<sup>14</sup> Another possibility would be to use non-uniform rational B-splines (NURBS) to approximate the surface. These spline surfaces are versatile objects for which the user has control over interpolation power as well as continuity and polynomial degree. They can be constructed simply and cheaply but require an affine map from a Cartesian parametric space in which the basis functions exist to physical space, so methods for properly constructing a mesh from the scan pattern would have to be explored further.<sup>7</sup> A third option very similar to NURBS are T-spline geometries. These may be advantageous because they are less restrictive on the scan pattern.<sup>20</sup> For all three approximation methods, the polynomial degree will control the accuracy (or lack thereof) of the approximation. The appropriate polynomial degree would have to be selected.

Table 13: Advantages and Disadvantages of Nodal Surface Approximation

Advantages	Disadvantages
Not restrictive on scan pattern	Strange behavior between interpolating points
Control over interpolation power/cost through approximation degree	Interpolation accuracy highly affected by points with large deviation

### 3.3.1.2 Modal Surface Approximation

Modal approximations utilize orthogonal bases to represent characteristic modes of a set of data. The most well-known of these types of methods comes from Fourier analysis. In this setting Fourier decomposition of the terrain map would give a notion of its contributing spatial frequencies, where high frequency modes represent sharp curves like object boundaries. The proposed method would filter the data in frequency space with an appropriately designed low-pass filter to eliminate these high order oscillations. Applying the inverse transform to the filtered data would yield a smooth, low-frequency representation of the ground. The cutoff frequency of such a filter would be determined by the characteristic size of the obstacles in the terrain being scanned, making this method highly application-specific. Additionally, the mathematics involved that transform between spatial and frequency domains are computationally heavy as they involve integration over the entire domain. The implications of these integration schemes on the pattern of the scan remains an area of research for the team. It may or may not be possible to compute these transformations over arbitrary orientations of points or it may be too computationally expensive.

Table 14: Advantages and Disadvantages of Modal Surface Approximation

Advantages	Disadvantages
Customizable for different hazard definitions by changing the cutoff frequency	Computationally expensive
Intuitive physical meaning (low-pass filter)	May not be possible over an arbitrary set of points

### 3.3.2 Gradient-Based Techniques

Gradient-based techniques look at the rate of change of height over the map. The local gradient can be calculated as simply the slope of a line connecting two neighboring points, or with more robust methods that weigh contributions from several surrounding points. Landing hazards will generate areas of high gradient, while smoother areas will have a low gradient. The success of these methods depends highly on the distribution of points and the connectivity between them<sup>2,17</sup>. Methods making efforts to negate this effect are well established and can be implemented relatively simply. The method of Delaunay triangulation will connect arbitrary organizations of points in two-dimensional space optimally for computing gradients.<sup>2</sup>

One of the limitations of these methods is that the gradients themselves do not account for the scale of what would be defined as a hazard. Height differences between closely spaced points may produce high gradient values, even if the height differences are small relative to the size of the lander. For this reason, a gradient-based algorithm would need to be supplemented with logic that accounts for the physical size of the high-gradient areas.

#### 3.3.2.1 Morphological Filter

The Morphological Filter is one of the simplest gradient-based techniques for hazard detection. It defines hazards based on the slope of lines connecting neighboring points. If the slope is above a given threshold, then the endpoints

can be marked as hazardous.<sup>16</sup> One implication of this is that each point has several slope values associated with it, rather than a single value that can be obtained with other methods by taking weighted values from surrounding points and combining those. The Morphological Filter would likely leverage the Delaunay triangulation for selecting neighboring points, and so it would lend itself well to an incoming stream of points.

Table 15: Advantages and Disadvantages of Morphological Filter

Advantages	Disadvantages
Simple software implementation	Information remains local, lacks a reference for absolute size of obstacles
Lends nicely to an incoming stream of points	

### 3.3.2.2 Kernel Convolution Filter

The Kernel Convolution Filter is a method with applications in image processing, where edges can be detected by finding areas of high color contrast. This method can be adapted to landing hazard detection by effectively treating the measured points as pixels with their height values as the corresponding “color.”

A small matrix, called a kernel, can then be convolved over each of the “pixels” to generate a value representing the local gradient at each point with values weighted from several neighboring points. In the analogy to pixels, this method works best when the ground-plane locations of the points form a uniformly distributed grid of squares. The method could be adapted to work with less-uniform scans, but this would likely require interpolation of measured data or would result in areas of low confidence where points are spaced more sparsely.

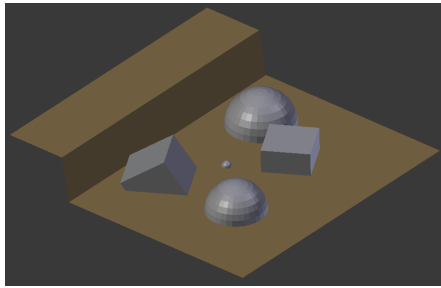
Following the gradient operation, another kernel could be used to smooth the resulting gradient map, delocalizing the slope information. This is a key process that helps counter the aforementioned difficulty with gradient-based methods. After the smoothing, a thresholding operation would designate areas of high gradient to be unsafe, and vice versa. This process has been implemented with high levels of success in the field of image processing.<sup>8</sup> For this project, the smoothing and thresholding could be tuned via testing to very accurately find obstacles in the field of view. Again, these techniques may be extended to point fields connected by Delaunay triangulations in the event that the scan pattern deviates too radically from a Cartesian grid.

Table 16: Advantages and Disadvantages of Kernel Convolution Filter

Advantages	Disadvantages
Highly proven in the field of image processing	Challenging to implement if scan pattern is not a Cartesian grid
Easy to implement	
Slope information can be delocalized	

### 3.3.2.3 Displaced Points Method

A less direct use of gradient techniques would be to look at the displacement of points from their expected positions on a flat plane. By looking at only the  $(x, y)$  locations (ignoring height data) of the points, obstacles and ground slopes could be identified by finding areas of closely or sparsely spaced points (see Figs. 13 & 14). This method relies heavily on prior knowledge of the scanning pattern and the ability to compare incoming point locations to expected location. This algorithm would create a map directly related to a gradient field without computing gradients. At this point similar smoothing and thresholding operations could be performed to identify objects.



**Figure 13:** Example terrain map in Blender

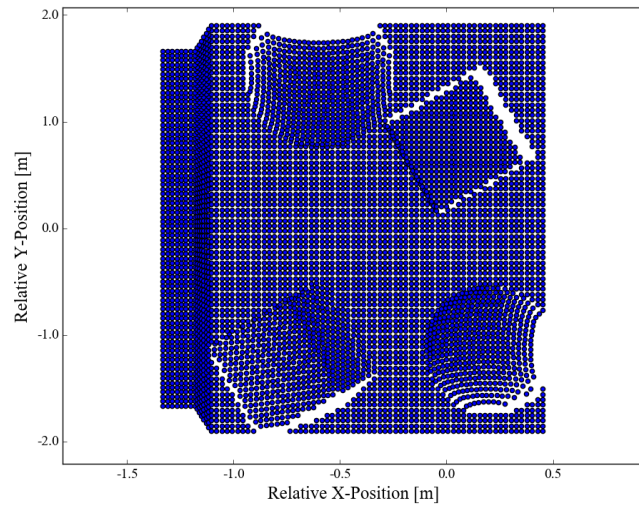


**Figure 14:** Resulting point distribution of simulated lidar scan

This algorithm shows promise because it leverages what has been a weakness in many of the other algorithms. Unfortunately the shadowing effect is only prevalent at high viewing angle so objects close to nadir may not be recognized as readily.

Table 17: Advantages and Disadvantages of Displaced Points Method

Advantages	Disadvantages
Leverages an issue in other methods: shadowing	Relies heavily on prior knowledge of the scanning pattern
Intuitive physical meaning (see above Figs.)	Will work less effectively close to nadir pointing

## 4 Trade Study Process and Results

In this section, the key design options from the previous section will be traded in order to select a baseline design.

### 4.1 Lidar Selection

#### 4.1.1 Criteria and Weighting

Table 18 shows the trade study parameters for the selection of the lidar sensor with the applied weights, driving requirements, and rationale for using each parameter.

Table 18: Lidar Trade Study Parameters

	Weight	Driving Requirements	Description and Rationale
<b>Sample Rate</b>	0.25	<b>DR 1.5, DR 1.4</b>	This parameter is simply the rate at which the type of lidar sensor can collect and transmit range data. This specification is heavily driven by requirement <b>DR 1.5</b> (time constraint) and requirement <b>DR 1.4</b> (required spatial resolution). The sample rate required to gather the minimum number of data points in 60 seconds based on <b>DR 1.4</b> is 100 Hz as shown in Appendix F. Sampling rates greater than 100 Hz are highly desirable to allow for data transfer, computation, and mechanism operation time. Any sampling rate greater than 400 Hz will allow for taking multiple range samples for each distinct scan location, while achieving the required spatial resolution. Since this parameter was derived from two design requirements needed to meet a strict functional requirement it received a weighting of 25%.
<b>Cross Range Error</b>	0.25	<b>DR 4.4</b>	Cross range error (defined in Appendix A) results from uncertainty in attitude measurements, lidar beam divergence, and lidar beam waist diameter. The maximum acceptable cross range error is 0.05m, putting an upper bound on how the above specifications can combine. The above specifications will also combine with angular position uncertainty in any peripheral scanning system. A high weighting of 25% was given to this parameter, as it is critical to meeting the overall mission objective of hazard detection.
<b>Range Error</b>	0.15	<b>DR 4.3</b>	All lidar sensors have a specified uncertainty in their range measurements, which is the dominant factor of the total error. A weighting of 15% was given to this parameter because it is the major contributor to meeting design requirement <b>DR 4.3</b> .
<b>Cost</b>	0.10	N/A	The project as posed is not feasible if a lidar sensor cannot be found that meets the design requirements placed on it. Therefore the cost of the sensor is not a significant driver as long as it fits inside the given budget. Spending a large portion of the budget on one sensor would however be a risky approach. A weighting factor of 10% was applied to reflect the desire of the team to mitigate this risk.

<b>Implications for Hazard Detection Algorithm</b>	0.10	<b>DR 1.5</b>	This parameter measures the ability of the lidar sensor to collect data in a method that is desired from the perspective of the hazard detection algorithm. Ideally sample points would be collected in a uniform spatial resolution regardless of the instantaneous angular position of the scanning system. A weighting of 10% was given, as this parameter will have an impact on computation time and complications, which are heavily restricted by requirement <b>DR 1.5</b> .
<b>Range</b>	0.10	<b>DR 1.3, DR 4.1, DR 4.2</b>	The operational range of the lidar sensor is governed by requirements <b>DR 4.1</b> and <b>DR 4.2</b> . A weighting of 10% was given to this parameter, as the constraint is easily met by sensors in each of the three design options to be traded. However, variation does exist when you pair operational range with other parameters that must be satisfied. For example lidar sensors with built in scanning generally have a lower maximum range than fixed or optically segmented sensors for the same cost.
<b>Moment of Inertia</b>	0.05	<b>DR 1.5</b>	None of the design options considered have the ability to scan in two dimensions, so the sensor must be actuated. The moment of inertia of the sensor will then have a minor impact on attainable scan rate, which is driven by functional requirement <b>DR 1.5</b> . This parameter can only be assessed comparatively for each design option considered. A weighting of 5% was applied, due to the fact that the implications can be addressed by scanning system design.

#### 4.1.2 Trade Study Scoring

Table 19 gives the metric for scoring each parameter in the trade study. Sample rate, cross range error, range error, and cost were categorized numerically based on their driving requirements. Algorithm implications, range, and moment of inertia were categorized in a qualitative manner.

Table 19: Lidar Sensor Parameter Metrics

Metric	1	2	3	4	5
<b>Sample Rate [Hz]</b>	< 100	100 - 199	200 - 299	300 - 399	> 400
<b>Cross Range Error [°]</b>	> 0.4	0.3 - 0.39	0.2 - 0.29	0.1 - 0.19	< 0.1
<b>Range Error [cm]</b>	> 4	3 - 3.99	2 - 2.99	1 - 1.99	< 1
<b>Cost [\$]</b>	> 4000	3000 - 3999	2000 - 2999	1000 - 1999	< 1000
<b>Algorithm Implications</b>	Impossible	Difficult	Undesirable	Inconvenient	None
<b>Range</b>	Operational Range does not meet requirements	N/A	N/A	N/A	Operational Range meets requirements
<b>Moment of Inertia</b>	Prohibitive	Large	Moderate	Small	Negligible

### 4.1.3 Trade Study

Table 20 provides the scores each design option was given for the selected parameters, and the cumulative total score. The results are discussed below.

Table 20: Lidar Sensor Trade Study

	Weight	Fixed Beam	Scanning	Optical Segmentation
Sample Rate	25%	3	5	1
Cross Range Error	25%	4	2	1
Range Error	15%	4	3	1
Cost	10%	4	3	5
Algorithm Implications	10%	5	4	2
Range	10%	5	1	5
Moment of Inertia	5%	2	3	4
Sum	100%	3.85	3.15	2.05

The sample rate parameter was simple to address, as each design option was researched to determine the typical sampling speed that could be expected. Cross range error was also simple to score for each design category, as described in Appendix A. The fixed lidars only had their specifications on beam divergence factor into the cross range error, whereas scanning and optically segmented sensors included additional sources of error. Scanning lidar's almost all had angular resolutions that were too low, or angular position uncertainty that were too high. The best cross range error that could be achieved with optically segmented sensors was  $0.15^\circ$  by  $0.3125^\circ$  (different in each dimension). The range error of each design option could again be assessed by checking the data sheets for sensors in each category to determine typical range errors. It was found that for like specifications, fixed, scanning, and optically segmented lidars scored a 4, 3, and 5 in the cost category respectively. Additionally, for like cost, fixed and optically segmented lidars were found that operated inside the required range, but considerably more money had to be spent to procure a scanning sensor that could operate with the same fidelity. For this reason scanning systems scored a 1 with the range parameter.

Algorithm implication was a more involved parameter to assess. Fixed lidar sensors placed no implications on the hazard detection algorithm, whereas scanning systems placed minor inconveniences, and optically segmented sensors resulted in complex scan patterns. For a scanning sensor, as the scan angle increases with a constant sample rate, the spatial resolution of the collected data would increase. This spatial resolution is bounded by requirement **DR 1.4**, which would be the resolution at the maximum scan angle. This results in tighter than required resolutions at all scan angles less than the maximum, and significant over sampling. The additional data would need to be filtered out, or combined with the expected data in some way, an additional task for the hazard detection algorithm. This required oversampling would also increase the required scan time. Fortunately scanning sensors characteristically have fast sample rates, where the over sampling would not have a significant impact on scan time. However, the increased number of unwanted points is an inconvenience. The smallest field of view per return for optically segmented sensors was  $0.3^\circ$  by  $2.5^\circ$ , well above the constraint in requirement **DR 4.4**. Eight of these segments are measured simultaneously, so it is conceivable to suggested that the field of views could be overlapped to obtain an average measurement of a smaller area. Eight overlaps would result in an identical sampling rate as a fixed beam sensor, so one potential benefit is negated, and unfortunately eight such overlaps only result in a reduced field of view of  $0.15^\circ$  by  $0.3125^\circ$ . The added complexity of overlapping paired with the additional load on the software side to track and combine the eight components of each desired measurement earned this method a score of 2.

Finally, the typical moment of inertia of each sensor was considered. One scanning design option being considered is mechanical actuation of the lidar itself. This actuation is governed by the fundamental equation  $\tau = I\alpha$ , where  $\tau$  is the torque required to achieve angular acceleration  $\alpha$  multiplied by the moment of inertia  $I$ . The torque required to control the motion of the sensor is directly proportional to the moment of inertia. Sensors with low moments of inertia

are desired, as less control authority will be required to operated the system. This results in a reduction of mechanical complexity, an increase in possible scanning rate, and a decrease in the cost of scanning system components. The optically segmented sensors were found to have a small moment of inertia. The typical fixed beam sensor being considered had moderate to small moments of inertia. Scanning sensors by themselves had small moments of inertia, but an additional factor had to be considered. The scanning systems feature a continuously rotating head, that possesses angular momentum. The scanning sensor must be rotated about a perpendicular axis to achieve a 2D scan. The angular momentum of the scanning head acts as rotational stiffness about the additional spin axis. This added stiffness earned the scanning sensors a score of 3.

The final score of each design option was separated by a significant amount. Fixed beam sensors scored a 3.85, 0.7 higher than the scanning sensors, and 1.8 points higher than optically segmented sensors. The superior specifications of the fixed beam sensors at similar price points make them the best space to explore for the final selection of the lidar sensor.

## 4.2 Scanning System Selection

Upon conducting the trade study for the lidar sensor, the importance of the scanning system trade has become clear. This selection process involved a trade study to quantitatively compare the various scanning system options. The following sections further describe the scanning options considered and the logic behind the scanning system trade study.

### 4.2.1 Criteria and Weighting

Table 21: Scanning System Trade Study Parameters

	Weight	Driving Requirements	Description and Rationale
<b>Cost</b>	0.1	N/A	In order to obtain sufficient pointing accuracy high quality motors and/or encoders will be needed. Such components vary greatly in price and can be quite expensive. Preliminary cost analysis shows that a large amount of the budget (possibly around 50%) will be dedicated to the scanning system. However, this same analysis showed that the scanning system should fit well within the budget. As a result, while still important, the cost was given a weighting of 0.1 which is less than other parameters more critical to functional requirements.
<b>Actuation Complexity for desired Scan Pattern</b>	0.2	<b>DR 3.2, DR 1.1, DR 1.2, DR 1.5, DR 4.5</b>	In order for the MACULA project to be deemed successful it must be capable of scanning (and analyzing) an area according to a pattern within sixty seconds. Systems that must be moved in a complex way during a scan will likely take much longer to complete a scan. Therefore, the complexity of actuation for desired scan patterns is important for achieving the functional and customer requirement that the system complete a scan in 60 seconds. As a result, this parameter was given a weighting of 0.2.

<b>Moment of Inertia of Rotating Components</b>	0.15	<b>DR 1.5, DR 4.4, DR 4.5</b>	The moment of inertia of the rotating components of the scanning system has a significant impact on many elements of the system as a whole. Namely, a system with a large moment of inertia will need much more powerful and expensive motors in order to move with the precision and accuracy mandated by the functional and design requirements. In particular, to complete a scan within 60 seconds a scanning system with a low moment of inertia will be advantageous in order to move rapidly while taking precise measurements. Nonetheless, a system with a large moment of inertia could be compensated for by using better motors. As a result this parameter was assessed a score of 0.15.
<b>Attitude Error</b>	0.2	<b>DR 4.4, DR 4.5</b>	Several important functional and design requirements are dependent on the pointing accuracy of the system. Since all the options traded in this study require actuation with motors, this parameter is intended to quantify how each system either magnifies or attenuates uncertainty inherent with the actuator angular position. When assigning scores for each system, it is assumed that the same motor system with the same angular uncertainty is used. The pointing accuracy significantly affects the cross range error and resolution limit for the system which is why it was assessed a higher weighting score of 0.2.
<b>Hardware Design Complexity</b>	0.1	<b>DR 1.1, DR 1.2</b>	This parameter is a measurement of how difficult it will be to design the scanning system from a physical standpoint. The two main aspects that make up this category are wiring and mechanical design. On the wiring side, the main concern is the use of rotating electrical components. On the mechanical side, this parameter is meant to assess the difficulty of mounting all components and designing/creating the physical scanning apparatus. This category was assigned a weighting of 0.1 since these tasks are not anticipated to be particularly difficult and many members of the team have experience in this field.
<b>Technology Readiness Level</b>	0.25	N/A	The most important trade parameter for the team is the readiness of these various scan technologies. Since this project is intended to be a novel proof of concept, it is unwise when designing the subsystems to use technology that is currently being researched. Advanced optical scanning systems may be advantageous for the project in some regards, however they likely would not be feasible for use within the scope of this class. Using technologies currently under development would put the project at risk of failing to achieve any scanning abilities. Due to this concern, this parameter was assigned a weighting of 0.25, the highest weighting of all parameters considered.

#### 4.2.2 Trade Study Scoring

Table 22: Scanning System Parameter Metrics

Metric	1	2	3	4	5
Cost	> 2000 USD	1500-2000 USD	1000-1499 USD	500-999 USD	< 500 USD
Actuation Complexity for Desired Scan Pattern	Uncontrollable	Complex	Moderate	Simple	Trivial
Moment of Inertia of Rotating Components	Prohibitive	Large	Average	Small	Negligible
Attitude Error with Constant $\delta$ in Motors	$\gg \delta$	$> \delta$	$\approx \delta$	$< \delta$	$\ll \delta$
Hardware Design Complexity	Overscoped	Involved	Moderate	Simple	Trivial
Technology Readiness Level	Research Based	Under Development	Made and Tested	Used in Real World Scenario	Commercial off the Shelf

#### 4.2.3 Trade Study

Table 23: Lidar Scanning Mechanism Trade Study

	Weight	Mechanical-Based	Mirror-Based	Risley Prisms
Cost	10%	2	4	4
Actuation Complexity for Desired Scan Pattern	20%	4	4	2
Moment of Inertia of Rotating Components	15%	2	4	5
Attitude Error with Constant $\delta$ in Motors	20%	3	1	4
Hardware Design Complexity	10%	2	3	4
Technology Readiness Level	25%	4	4	3
<b>Sum</b>	100%	3.1	3.3	<b>3.5</b>

To determine a suitable technology for the scanning system in project MACULA, a linear trade study was conducted that compared mechanical, optical mirror, and Risley-Prism-based systems, as seen in Table 23 on ratings of 1 – 5. The trade study compared the cost, actuation complexity, moment of inertia, attitude error, design complexity and

technology readiness level of each system with corresponding weights in table 21 . This resulted in scores of 3.1, 3.3, 3.5 for the mechanical, optical mirror, and Risley Prism systems, respectively.

The first major metric that was considered in the scanning system trade study was cost. Preliminary cost analysis revealed an upper limit of \$2000 for the scanning system budget. Ranges of cost were then assigned to each rating and compared to the average costs of each system overall. Mechanical, optical mirrors, and Risley Prisms received scores of 2, 4, and 4, respectively. In considering each system overall, the preliminary cost analysis of each system examined the potential price of each component. Thus, due to being a system with high inertia, the mechanical system would require stronger and more accurate actuating systems that are quite expensive, earning it a score of 2. The optical mirror and Risley Prism systems, however, proved to be less expensive. Both optical mirrors and Risley Prisms are fairly inexpensive, ranging in prices from tens to several hundreds of dollars for systems that meet the requirements, and did little to factor into the pricing. They would also require potential actuators of similar quality and ultimately price, earning them both scores of 4.

When considering each of these systems the actuation complexities for desired scan patterns must be considered. Scores of 4, 4, and 2 were assigned to the mechanical, optical mirror, and Risley Prism systems, respectively. This metric considers the difficulty and complexity of actuating these systems such that they can complete a given scan pattern. The mechanical system earned a score of 4 due to the possible simplicity of the system. It is capable of steering the lidar beam to any commanded angle in nearly any desired pattern. However, angular rates and positioning with respect to the actuating method is still required, thus a score of 4. The optical mirror system is fairly simple due to the law of reflectivity. By knowing the angle of the beam with respect to the mirror surface, the mirror configuration can be manipulated to move the beam in a variety of configurations. Where the optical mirrors suffer, however, is when using multiple mirrors the process of beam path manipulation becomes much more involved due to needing to know the relative path of the beam with respect to each mirror. This complexity earned the optical mirror system a score of 4. For Risley prisms, the scanning dynamics involved would be complicated and actuating them to achieve such a scan would be difficult and time costly. The prisms themselves are limited in possible scan patterns, and these patterns themselves are difficult to achieve, earning the system a score of 2.

In order to examine possible scan times for each system, the possible moments of inertia needed to be actuated were examined. The individual rankings were based off of the equation for torque,  $\tau = I\alpha$ , and assuming that each system would be actuated at the same angular acceleration,  $\alpha$ . Scores of 2, 4, and 5 were assigned to the mechanical, optical mirror, and Risley prism systems, respectively, off of the metrics in Table 22. Mechanical systems received a score of 2 due to the majority of systems being quite large and heavy, thus having a large moment of inertia,  $I$ . The higher moment of inertia would require a larger torque from the actuating mechanic in order to manipulate the structure through out a given scan pattern, and would affect the time to scan due to overshoot and potentially increase the scanning error. The mirrors and Risley prisms used within their respective systems, however, are much smaller by comparison and resulting in much lower inertia. The average optical mirror weighed a more than a prism, whose weight is nearly negligible, thus the two systems received scores of 4 and 5, respectively.

The attitude error for the different scanning systems was analyzed next. When computing this error, the error resulting from the motors was assumed to be held constant. The mechanical system, mirror system, and Risley Prism system earned scores of 3, 1, and 4 respectively. Assuming good motors and encoders, the mechanical system would be able to achieve an attitude error that would not compound upon the error from the motors. This allowed the mechanical system to earn a 3. Due to the law of reflectivity, the two mirror system would quadruple the error of the motors. This drastic increase in error resulted in giving the mirror system a 1 in this category. The Risley Prisms, on the other hand, would actually minimize the error from the motors; thus, it earned a score of 4.

The hardware design complexity was analyzed to determine how difficult it would be to build the system. This trade looked at whether the system would be overscoped, involved, moderate, simple, or trivial; these options were then assigned a rating from 1 to 5 respectively. Based on this criteria the mechanical system, mirror system, and Risley Prism system were given scores of 2, 3, and 4 respectively. Since the mechanical system would have to actuate the whole lidar, the lidar would have to be perfectly placed on the system in order to ensure accurate results. Also, the hardware would be bulky and would add unnecessary mass to the system. Thus the mechanical system received a score of 2. The mirror system on the other hand, would not require as much hardware since it would only need to actuate the mirrors as opposed to the entire lidar. Therefore, the mirror system received a score of 3. Since the Risley Prisms are less optically complex than the mirror system, they received the best score with a 4.

The technology readiness levels of the three scanning systems were analyzed to determine which of the three design options was feasible. For the purpose of this trade study, what could be done within the scope of this class was also factored in. The trade study looked at whether the option was research based, under development, made

and tested, used and tested in real world scenarios, or commercial off-the-shelf; these options were then assigned a rating from 1 to 5 respectively. The mechanical system, mirror system, and Risley Prism system received scores of 4, 4, and 3 respectively. Since mechanical systems and mirrors have been used in real world scenarios to steer optical beams, they both earned a score of 4. Risley Prism systems, on the other hand, are still undergoing testing in industry. Therefore, a score of 3 was assigned to Risley Prisms.

#### 4.2.4 Mirror/Gimbal Hybrid

After analyzing the scanning system trade study results, it was noticed that the mirror and mechanical based scanning systems were mutually complimentary, so a mirror/gimbal hybrid conceptual design was added to the scanning system selection analysis. A mirror/gimbal hybrid system would achieve 2-D scanning with a mirror based system in one dimension and a mechanical based system in the other. The beam could thus be steered by moving the mirror with a gimbal in two dimensions. An example a mirror/gimbal hybrid system is shown below in Fig. 15.



**Figure 15:** Example of gimbal mirror hybrid system. Image obtained from Aerotech Inc.<sup>1</sup>

A system such as this would benefit from several of the individual advantages correlated with mirror based and gimbal based systems. The cost of a mirror/gimbal hybrid system would likely be less than that of a pure gimbal system since cheaper, less powerful motors could be purchased. In addition, the actuation complexity for a desired scan pattern would be simpler than a pure mirror system since a mirror/gimbal hybrid system can function using only one mirror. The moment of inertia of rotating components would also be an advantage because mirrors have a smaller moment of inertia in comparison to the platforms needed with a gimbal system. Another advantage of a mirror/gimbal system would be in attitude error. The attitude error with one mirror is half that of a system with two mirrors by reason of the law of reflectivity. While still not as low as the attitude error for a pure gimbal system this is certainly an improvement when compared to a pure mirror system. For hardware design complexity, a mirror/gimbal system would be an improvement on a gimbal system due to the fact that slip rings could likely be avoided (although a different design than is pictured in Fig. 15 would be needed). At last, the technology readiness level would be essentially unchanged as mirror/gimbal hybrids have also been built in used many times before. All in all, a mirror/gimbal hybrid system improves upon either a pure gimbal or mirror based system in nearly every category. For this reason,<sup>1</sup> the scanning system trade study was repeated with a mirror/gimbal hybrid included.

#### 4.2.5 Trade Study with Mirror/Gimbal Hybrid

Table 24: Lidar Scanning Mechanism Trade Study

	Weight	Mechanical Based	Mirror Based	Risley Prisms	Mirror/Gimbal Hybrid
Cost	10%	2	4	4	4
Actuation Complexity for Desired Scan Pattern	20%	4	4	2	4
Moment of Inertia of Rotating Components	15%	2	4	5	4
Attitude Error with Constant $\delta$ in Motors	20%	3	1	4	2
Hardware Design Complexity	10%	2	3	4	3
Technology Readiness Level	25%	4	4	3	4
<b>Sum</b>	100%	3.1	3.3	<b>3.5</b>	3.4

In review of these results it is evident that the mirror/gimbal system is an improvement over both the pure gimbal and mirror systems. Nonetheless, the Risley Prism system still has a slight advantage. This advantage is small enough that either option could be reasonably chosen. For cost, the mirror/gimbal system earned the same score as the pure mirror system. As far as actuation complexity for desired scan pattern, the mirror/gimbal hybrid earned the same score as the pure mechanical system since only one mirror is involved. For moment of inertia of rotating components, the gimbal/mirror system earns the same score as the mirror system since the size of the gimbal part of the system will be reduced by using a mirror. For attitude error, the mirror/gimbal hybrid earned a score of 2 since the error is less than a pure mirror system but greater than a pure mechanical system. For hardware complexity, the mirror/gimbal system received the same score as a mirror system since the use of a slip ring could be avoided. At last, the mirror/gimbal hybrid system got a technology readiness level score of 4 because mirror/gimbal hybrids have been used and tested to a similar extent as pure mirror and gimbal based systems.

### 4.3 Software Selection

#### 4.3.1 Criteria, Weighting, and Scoring

The following table outlines the algorithm attributes that are important to determination of a hazard detection scheme. These attributes are given a weight along with justification and the quantitative measure used to score the algorithms in that category.

Table 25: Sensitivities and Justification for Algorithm Selection Criteria

	Weight	Driving Requirements	Description and Rationale
<b>Computational Complexity</b>	0.1	<b>DR 1.5</b>	The algorithms must not be prohibitively slow but it is expected that computation will not be the limiting factor compared to the time taken to complete the mechanical scan. Algorithms with low computational complexity will be given a high score. Algorithms are ranked comparatively, meaning the cheapest algorithm will receive a 5, and score will decrease as integers with increasing number of necessary operations.
<b>Robustness</b>	0.65	<b>DR 7.1</b>	The entire success of the system beyond success level 2 hinges on the robustness of the hazard detection algorithm. The system must be able to accurately detect hazards. Five unit tests were developed and can be found in Fig. 38 through Fig. 42 in Appendix E. The score in this category is the number of unit tests for which a particular algorithm was expected to accurately identify hazardous and safe zones. It was assumed that the feature could be resolved well enough that failure would be due to the algorithm itself rather than the scanning system.
<b>Calculation with Incoming Point Stream</b>	0.1	<b>DR 7.1</b>	In an actual real-time application, the ability to perform map analysis in parallel with the mechanical scan is valuable because the scan can terminate if a safe zone is found early enough. Algorithms that require the entire set of measurements will be given a 1. Algorithms that depend on local neighboring points but not the entire grid will be given a 3. Algorithms that do not leverage relationships between points will be given a 5.
<b>Low Impact on Mechanical System</b>	0.15	<b>DR 1.1, DR 1.4</b>	Because the subsystems depend on each other, a good algorithm will allow the scanning subsystem to complete its task in an arbitrary fashion. An algorithm that requires very specific scanning capabilities from the mechanical subsystem may result in unnecessary tall poles associated with the design and construction of the scanning system. Algorithms that rigidly require a specific grid pattern receive a score of 1. Algorithms that work better with specific grid patterns but can be adapted to arbitrary patterns receive a 3. Algorithms agnostic to the scan pattern receive a score of 5.

### 4.3.2 Trade Study

Table 26: Algorithm Trade Study

	Weight	Simple Filter	Surface-Based Filter	Morphological Filter	Fourier Decomposition	Image Processing	Point Displacement
<b>Computational Complexity</b>	10%	5	3	4	2	4	5
<b>Robustness</b>	65%	1	3.5	5	3.5	5	4
<b>Calculation with Incoming Point Stream</b>	10%	5	1	5	1	3	5
<b>Low Impact on Mechanical System</b>	15%	5	5	3	3	3	5
<b>Sum</b>	100%	2.4	3.425	4.6	3.025	4.4	4.35

The scoring in this table comes directly from the scoring guidelines outlined in Table 26 and the unit tests in Appendix E. See Appendix E for more details on which unit tests for robustness were passed by which design options.

First it should be noted that the simple filter received the worst score by far, verifying the choice of weights in the trade. The smoothing algorithms both received a low score which is reasonable considering their relatively high computational complexity and inability to perform continuous map analysis. Of course robustness was weighted most heavily and the smoothing algorithm's perceived failure on the unit tests hurt them the most. The remaining options received similar scores. Moving forward, these methods will be scrutinized and tested. They all employ similar techniques and it would be reasonable to assume that the final algorithm will draw on concepts from all three of these in order to leverage their strengths.

## 5 Selection of Baseline Design

The results of each trade study have been presented in the previous section. In this section, these results will be evaluated and a description of the baseline design will be presented.

The fixed-beam lidar won the trade study with a score of 3.85, compared with 3.15 and 2.05 for scanning lidar and optically segmented lidar respectively. The success of the fixed-beam lidar in this trade study was largely due to the fact that it allows for a custom scanning system to be constructed, rather than being included with the selection of the lidar sensor. Both scanning lidar and optically segmented lidar are heavily constrained in terms of scan pattern and cross range error, and these constraints were found to be prohibitive for the project. The fixed-beam lidar won by a margin of 0.7, above the 10% required for confidence in the result. Thus, a fixed-beam lidar was selected for the baseline design.

The scanning mechanism trade study was less decisive. The Risley Prism system won the trade study with a score of 3.5, over mechanical-based and mirror-based with scores of 3.1 and 3.3 respectively. The success of Risley Prisms in this trade study can be attributed to the low moment of inertia of rotating components and the low hardware design complexity. However, the results of this trade study were not conclusive, as the margin of victory was under 10%. Thus, another trade study was conducted, adding a mirror/gimbal hybrid system into the design option space. It was determined that many of the pros of mechanical-based and mirror-based systems did not overlap, so a hybrid may allow for the "best of both worlds". This new mirror/gimbal hybrid technology was evaluated against the three original options, earning a score of 3.4. Thus, mirror/gimbal hybrids perform slightly better than mechanical-based or mirror-based systems alone, but not by a decisive margin. The final result of this trade study is that Risley Prisms are the most promising option for the baseline design, but other options cannot yet be ruled out. A major drawback

to Risley Prisms is that the TRL is relatively low and that the team has little experience with the complicated optics. Going into Preliminary Design Review (PDR), Risley Prism systems will be further investigated through preliminary design and modeling in order to determine their feasibility. A mirror/gimbal system will be used as an “off-ramp” at the PDR stage, pending the results of the feasibility analysis for Risley Prisms.

Finally, the software baseline design must be selected. Six different options for hazard detection algorithms were considered, receiving scores ranging from 2.4-4.6. The morphological filter has won the trade study, but image processing and point displacement are within the 10% margin of uncertainty. Unlike the lidar sensor or the scanning system, the hazard detection software can be modified as the project goes forward. As preliminary design is conducted and prototype algorithms are coded and tested, it is not unreasonable that several of these top-scoring methods can be effectively combined. The analysis required to determine the exact combination of methods for the ideal algorithm is beyond the scope of this document. The most logical choice for the preliminary design is the top-scoring option: morphological filter. However, as has been stated, other scores were close to the winning score, so these options will be carried through into preliminary design.

In summary, the baseline design will consist of a fixed-beam lidar sensor whose beam will be directed by a Risley Prism system. The resulting data will be analyzed for hazards using a morphological filter. Entering preliminary design, these design options will be tested for feasibility, and if necessary, second and third place finishers will be used as “off-ramps.”

## Memorandum on Test Options

A major piece of feedback on MACULA’s Project Definition Document was the lack of a discussion on test. Due to the nature of this project, test will be a challenging and important component of project success. This memorandum will summarize the team’s progress on test planning.

The 15m range requirement will need to be verified using a full scale test, which will require at least a 15m space. For a direct verification of the requirement, this test should be conducted vertically, with the system looking down on the test terrain. However, a horizontal test can also verify this requirement, and may be easier to conduct. Instead of needing a 15m vertical space (close to five stories), a 15m horizontal space will be required. Scanning system actuation is the only major component of the project that may be affected by a change in orientation from vertical to horizontal. If a Risley Prism system is implemented, a horizontal orientation will have little effect on the system due to the low inertia of the actuated components. However, if a mirror/gimbal hybrid system is implemented, care will be taken to ensure that components rotate about their center of gravity, eliminating the effect of the horizontal test on the performance of the system.

Several locations have been identified as potential test sites, both for vertical and horizontal tests. The RECUV facility in the Fleming building is not 14.1m tall, but could be used for a scaled vertical test (more on this in the next paragraph). This facility could also be used for a horizontal test, and is desirable because of the contained, indoor nature of the space (more on this in the next paragraph). Professor Farsworth’s wind tunnel building on East campus is another potential location for a horizontal test, and is desirable for the same reasons as the RECUV facility. In order to conduct an indoor 14.1m vertical test on campus, the athletic department facilities may be appropriate. For example, Coors Events Center and the Balch Fieldhouse have large vertical open spaces with infrastructure to facilitate the mounting of the system. Neither of these locations has been measured, but they will be further investigated in the future. Horizontal and vertical outdoor test locations include the engineering center roof (vertical), and any building wall on campus (horizontal). An outdoor test has significant disadvantages if the system is not eye-safe. It is also worth noting that tests are not restricted to strictly horizontal or vertical orientations. Matt Rhode will be the most important personnel resource going forward in selecting and obtaining test locations, and the team plans to work closely with him before pursuing outside assistance.

Indoor test locations have the distinct advantage that they are more contained and controllable. If the selected lidar sensor is not eye-safe, significant care will be given to controlling the test area and keeping un-protected personnel out of the minimum safe distance. With this in mind, indoor test locations are more desirable, but outdoor test locations have not been ruled out.

It is also worth mentioning the applicability of a scale test. In order to fulfill all of the requirements, at least one test at the full 14.1m must be conducted to verify the full capabilities of the system. However, many tests can be performed at a shorter distance. This will make test logistics simpler, as a full scale test location must only be used for several days. Another challenge associated with a full scale test is the size of the scanned area. At a 14.1m range,

the scanned area will have a maximum diameter of 5.13m. Building a mockup of this size is unfeasible. However, the requirements can still be fully verified using a smaller mockup at the full 14.1m and only verifying the output of the algorithms over this smaller known terrain. This smaller mockup can be moved within the full scan area to verify that the system satisfies requirements at all scan angles from nadir to 20°.

Going forward, more thought will be given to all of these options. Test was not included in any trade studies because all of the baseline options are equally testable. Entering the PDR stage, more consideration will be given to the testability of designs.

## References

- [1] “AMG Series Optical Mounts & Gimbals.” Aerotech. Aerotech Inc., n.d. Web. 22 Sept. 2016. <<https://www.aerotech.com/product-catalog/gimbals-and-optical-mounts/amg.aspx>>.
- [2] Berg, Mark . Computational Geometry: Algorithms and Applications. Berlin: Springer, 2008. Print.
- [3] By FAS — March 23, 2016. “Federation Of American Scientists -.” Federation Of American Scientists. N.p., n.d. Web. 24 Sept. 2016.
- [4] Cryan, Scott, and Christian, John A. “A Survey of LIDAR Technology and its Use in Spacecraft Relative Navigation.” AIAA Guidance, Navigation, and Control (GNC) Conference, Boston, MA, 19-22 Aug. 2013. Web.
- [5] Dunbar, Brian. “Lidar Atmospheric Sensing Experiment (LASE): Measuring Water Vapor, Aerosols and Clouds.” NASA. NASA, 21 Nov. 2004. Web. 24 Sept. 2016.
- [6] Folger, Jean. “Why Curiosity Cost \$2.5 Billion.” Investopedia, LLC. 5 Sept. 2012. Web.
- [7] Hughes, T. J. R, J. Cottrell A., and Y. Bazilevs. “Isogeometric Analysis: CAD, Finite Elements, NURBS, Exact Geometry and Mesh Refinement.” Computational Methods in Applied Mechanics and Geometry 194.39-41 (2005): 4135-195. Web.
- [8] Gonzales, Rafael C. Digital Image Processing. 3rd ed. N.p.: Pearson Education International, n.d. Print.
- [9] “LeddarTech Launches LeddarVu, a New Scalable Platform Towards High-Resolution LiDAR.” PR Newswire Association LLC. Quebec City, 7 Sept. 2016. Web.
- [10] “LiDAR, Laser Scanners and Rangefinders.” RobotShop, Inc. 2016. Web. <<http://www.robotshop.com/en/lidar.html> >
- [11] Lynch, Andrew, and Kai Focke. “Beam Manipulation: Prisms vs. Mirrors.” Photonik International (n.d.): n. pag. Mar. 2009. Web. 20 Sept. 2016. <<http://www.edmundoptics.com/globalassets/resources/articles/beam-manipulation-prisms-vs-mirrors-en.pdf>>.
- [12] “Puck LiDAR: Our Lightest Yet.” Velodyne LiDAR, Inc., 2016. Web. <<http://velodynelidar.com/vlp-16-lite.html>>
- [13] “Round Wedge Prisms.” Round Wedge Prisms. THORLABS, n.d. Web. 20 Sept. 2016. <[https://www.thorlabs.com/NewGroupPage9.cfm?ObjectGroup\\_ID=147](https://www.thorlabs.com/NewGroupPage9.cfm?ObjectGroup_ID=147) >.
- [14] Saniee, Kamron. “A Simple Expression for Multivariate Lagrange Interpolation.” SIAM (2007): n. pag. Web.
- [15] Schwarze, Craig. “A New Look At Risley Prisms.” Photonics Spectra (n.d.): n. pag. Photonics Media, June 2006. Web. 20 Sept. 2016.
- [16] Shan, Jie, and Charles Toth K. Topographic Laser Ranging and Scanning: Principles and Processing. Boca Raton: CRC/Taylor & Francis Group, 2009. N. pag. Print.
- [17] Shewchuk, J. “What is a good linear finite element? interpolation, conditioning, anisotropy, and quality measures (preprint).” University of California at Berkeley 73 (2002).
- [18] “Technology Overview.” Advanced Scientific Concepts, Inc. 2015. Web. <<http://www.advancedscientificconcepts.com/technology/technology.html> >
- [19] Wilsenack, Frank. “Defense & Security.” Detecting and Tracking Thin Aerosol Clouds. SPIE, 12 Oct. 2012. Web. 24 Sept. 2016.
- [20] Y. Bazilevs et al., Isogeometric analysis using T-splines, Comput. Methods Appl. Mech. Engrg. (2009), doi:10.1016/j.cma.2009.02.036

## Appendix

### A Deriving Allowable Angular Position Uncertainty

#### A.1 Setting the Scene

The maximum cross range error is bound to  $0.05m$  by requirement **DR 4.4**. This can be used to derive the total allowable angular position error for the scanning system, which is a function of the attitude measurement uncertainty as well as the beam diameter and beam divergence of the lidar sensor. Fig. 16 was developed in conjunction with Dr. Thayer for previous research, and depicts the described problem, excluding the beam diameter. The situation is identical for the application of this project. The maximum slant angle and distance of  $20^\circ$  and  $15\text{ m}$  respectively will be substituted for bank slope and target distance. The resulting range and cross range error will be derived as a function of the angular position uncertainty and laser beam divergence.

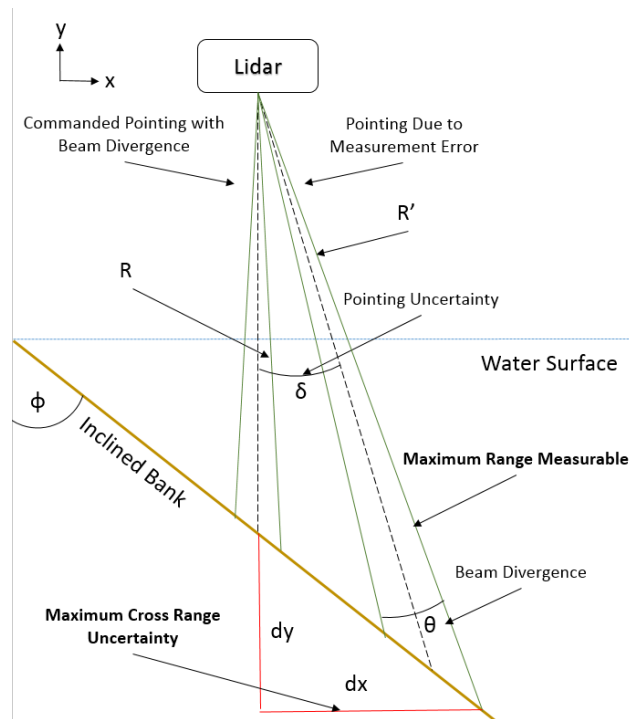


**Figure 16:** Scene depicting angular position geometry for bathymetry measurements

#### A.2 Deriving the Governing Equations

Fig. 17 depicts the geometry of the problem. The quantities shown are the system's angular position uncertainty,  $\delta$ , distance to target,  $H$ , and target bank slope,  $\phi$ . We wish to calculate the cross-range error,  $dx$ , and measured distance to target error,  $dr$ , which can both be directly calculated from the three known quantities. The desired cross-range error is orthogonal to the commanded pointing, which takes the place of the y-axis.  $H'$  and  $r'$  are new lengths that are created by finding the intersection of the bank slope and maximum pointing uncertainty, and then extending a line from this point to the intended target line so that they meet at a ninety degree angle. This generates two right triangles that will be used to directly calculate  $dr$  and  $dx$  from the three known quantities.

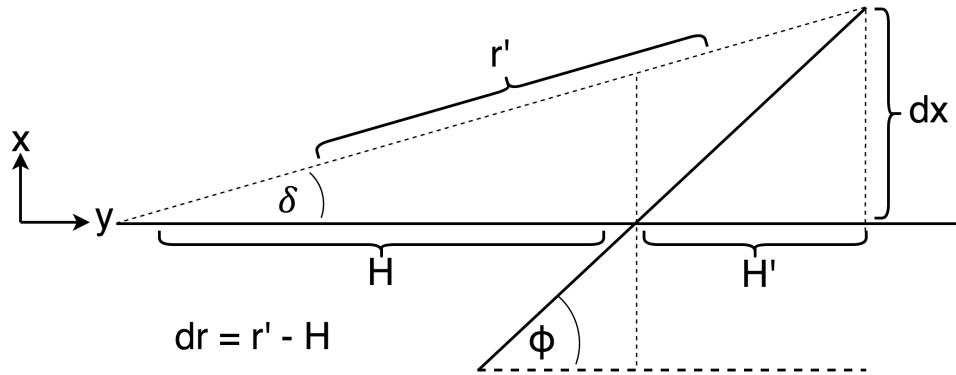


**Figure 17:** Problem Geometry

First, an expression for the cross range uncertainty,  $dx$  in terms of  $\delta$ ,  $\phi$ , and  $H$  will be derived. This is started by presenting the trigonometric tangent relations of the two triangles, which is shown below in equation 1

$$\tan(\delta) = \frac{dx}{H + H'} \quad \text{and} \quad \tan(\phi) = \frac{dx}{H'} \quad (1)$$

Solving the right hand side of equation 1 for  $H'$  and substituting it into the left and side of the same equation yields equation 2 shown below.

$$\tan(\delta) = \frac{dx}{H + \frac{dx}{\tan(\phi)}} \quad (2)$$

Multiplying equation 2 by the denominator of the right hand side, and then moving all  $dx$  parts back to the right side yields equation 3.

$$H \tan(\delta) = dx - \frac{dx \tan(\delta)}{\tan(\phi)} \quad (3)$$

Factoring out and solving for  $dx$  produces equation 4, which can be simplified to equation 5. We now have the cross range error as function of three known quantities.

$$dx = \frac{H \tan(\delta)}{1 - \frac{\tan(\delta)}{\tan(\phi)}} \quad (4)$$

$$dx = \frac{H \tan(\delta) \tan(\phi)}{\tan(\phi) - \tan(\delta)} \quad (5)$$

Next an expression for the range uncertainty must be derived. First the trigonometric cosine relation is presented and the value of  $H'$  is substituted into this cosine relation, which is shown below in equation 6.

$$\cos(\delta) = \frac{H + H'}{r'} \quad \text{and} \quad H' = \frac{dx}{\tan(\phi)} \quad \text{thus} \quad \cos(\delta) = \frac{H + \frac{dx}{\tan(\phi)}}{r'} \quad (6)$$

We can then solve for  $r'$  and substitute in the previously derived expression for  $dx$  which cancels the  $\tan(\phi)$  denominator of the  $dx$  term.

$$r' = \frac{H + \frac{H \tan(\delta)}{\tan(\phi) - \tan(\delta)}}{\cos(\delta)} \quad (7)$$

Multiplying the lone H by  $\frac{\tan(\phi) - \tan(\delta)}{\tan(\phi) - \tan(\delta)}$  produces equation 8, which simplifies to equation 9.

$$r' = \frac{H \tan(\phi) + \left( H \tan(\delta) - H \tan(\delta) \right)}{\cos(\delta)(\tan(\phi) - \tan(\delta))} \quad (8)$$

$$r' = \frac{H \tan(\phi)}{\cos(\delta)(\tan(\phi) - \tan(\delta))} \quad (9)$$

As shown in Fig. 17  $dr = r' - H$ . The final expression for the maximum range error is shown below in equation 10, and is in term of the same known quantities.

$$dr = \frac{H \tan(\phi)}{\cos(\delta)(\tan(\phi) - \tan(\delta))} - H \quad (10)$$

Some beam divergence  $\theta$  can be included in this error calculation, by simply replacing  $\delta$  with  $\delta + \frac{\theta}{2}$  in both equation 5 and 10. Re-examining Fig. 16 one can see that the beam divergence creates an ellipse of possible return locations, which is extended when the system's pointing is perturbed by the maximum angular position uncertainty  $\delta$ . The maximum difference between measurable ranges cross-ranges can be obtained by adding the equations 5 and 10 with  $\delta$  first replaced by  $\frac{\theta}{2}$  and then by  $\delta + \frac{\theta}{2}$ . This is shown by equations 11 and 12.

$$dx_{max} = \frac{H \tan(\frac{\theta}{2}) \tan(\phi)}{\tan(\phi) - \tan(\frac{\theta}{2})} + \frac{H \tan(\delta + \frac{\theta}{2}) \tan(\phi)}{\tan(\phi) - \tan(\delta + \frac{\theta}{2})} \quad (11)$$

$$dr_{max} = \frac{H \tan(\phi)}{\cos(\frac{\theta}{2})(\tan(\phi) - \tan(\frac{\theta}{2}))} + \frac{H \tan(\phi)}{\cos(\delta + \frac{\theta}{2})(\tan(\phi) - \tan(\delta + \frac{\theta}{2}))} - 2H \quad (12)$$

### A.3 Special Cases

Two special cases arise, one that requires new derivations, and another that is non-physical but generated by the assumed geometry. If  $\phi$  in 17 is equal to 90 degrees, equations 5 and 10 break down because the  $\tan(90)$  is undefined. The geometry in this case is simplified however, as the right hand triangle vanishes and the trigonometric relations of the full triangle can be used. Equation 13 shows the cross range and range uncertainty in this case.

$$dx_{\phi=90} = H \tan(\delta) \quad \text{and} \quad dr_{\phi=90} = \frac{H}{\cos(\delta)} - H \quad (13)$$

Next we simply must require that  $\phi$  is never less than or equal to  $\delta$ . As  $\phi$  approaches  $\delta$ , the target's slope and the angular uncertainty line approach a parallel relationship, resulting in a  $r'$  that grows to infinity. The range and cross-range error in this situation would mathematically grow to infinity, which is the desired physical behavior. As  $\phi$  falls below  $\delta$  and goes to zero, the geometry flips, and  $r'$  approaches zero. This is not the desired physical behavior. In this case the assumed geometry no longer applies, and the two lines continue to never intersect. In reality this and the parallel case would result in failing to hit the target at all.

### A.4 Applying the Mathematics to the Conceptual Design

The maximum scan angle and slant range of 20° and 15m can be translated directly into  $\phi$  and H. The above equations were transferred into MATLAB, and used to generate contour plots showing the range and cross range error as a function of target range and total angular uncertainty. Fig. 18 and Fig. 19 show the results.

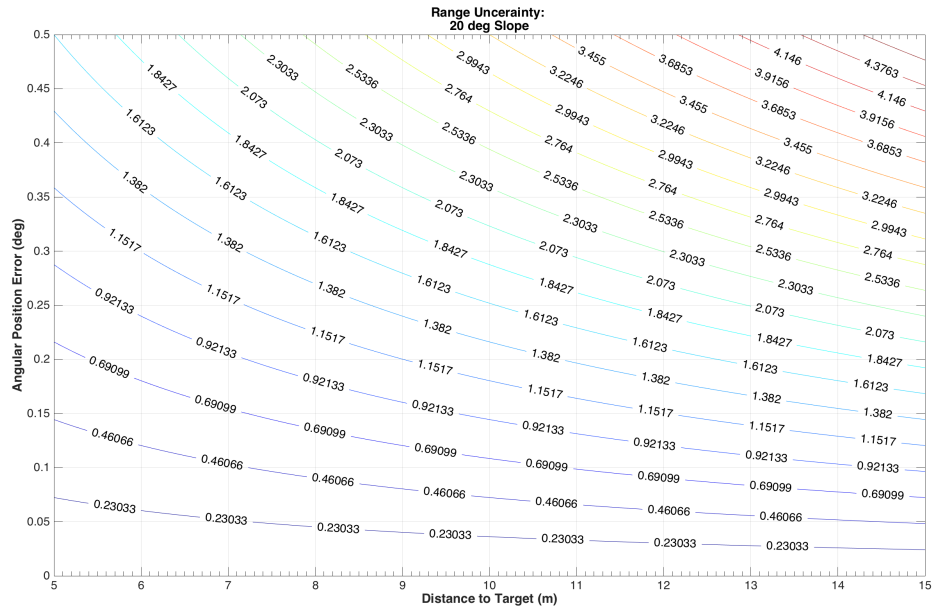


Figure 18: Range error contours

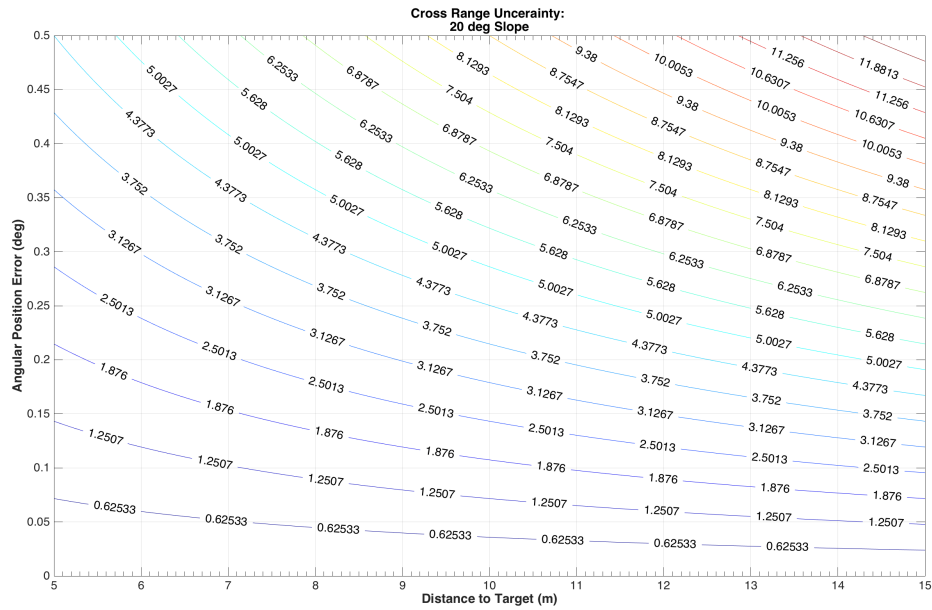


Figure 19: Cross range error contours

## B Translation of Range and Angular Position Information to Points in Inertial Space

### B.1 Overview

The objective of this section is to derive a generalized equation for an absolute range reading from a two axis gimbale lidar system. The azimuth axis will be defined as the spin axis that is aligned with the local vertical direction, which is commonly referred to as the yaw axis. The pitch axis is defined as the spin axis which is aligned with the local horizontal direction. The term pitch plate will be used to describe the platform to which the lidar sensor is attached, and is the the physical plate that is gimbale in two axes. Generalized geometry will be defined and then vectorized to support the developed mathematics. Co-rotating frames will also be defined. The formulated mathematics will result in a governing equation for an absolute position vector from a system origin to a target in inertial coordinates as a function of the pitch angle,  $\phi$ , yaw angle,  $\psi$ , and lidar measurement,  $R$ . This vector represents the three dimensional position of the target relative to the system origin. Other parameters included in the equation will be geometric constants. Thus the governing equation can be used for any two axis gimbale lidar system.

### B.2 Factors Leading to a More Complex Transformation than Spherical to Cartesian Coordinate Frames

A two axis gimbale platform can be rotated about two axes. If exceptional care is placed in the fabrication and integration of the system structure, the azimuth and pitch axes will intersect at some point in space. Ideally the lidar detector should be placed at exactly this point such that it is only rotated and experiences no translation. In this situation the absolute range measurements along with  $\phi$  and  $\psi$  take the form of a spherical coordinate system, which is trivially transformed into a Cartesian representation. Many factors lead to deviations from this ideal situation.

Firstly the pitch and azimuth axes are not required to intersect, leading to translation of the pitch axis around the azimuth axis, and the removal of a single rotational origin. Secondly the exact location of the detector within the lidar system may not be perfectly known, making it impossible to ensure that it will not experience any translation. Additionally a lidar system is usually fixed to a plate that is gimbale, making it awkward or exceptionally difficult to perfectly position the system.

These factors combine to create a somewhat complicated dynamical system, where the position of the lidar detector is a function of the pitch and yaw angles. This position must be accounted for when translating lidar measurements into a three dimensional map, as if the position is ignored the resulting map will be warped. The magnitude of this warping effect depends only on the geometry of any given system, and derivation of an equation that accounts for the previously discussed factors is possible.

### B.3 Pitch Plate Geometry

Fig. 20 defines all necessary geometry of the pitch plate for a general system.  $O_g$  is the geometric origin of the physical pitch plate, and can be found by measuring the outer dimensions of the plate.  $L$  is the position of the lidar detector relative to  $O_g$ , where  $R_{L/O_g}$  is the vector describing this position. For any given system  $R_{L/O_g}$  will be known to varying degrees of accuracy, but for now it will be assumed to be exactly known. The X, Y, Z, coordinate frame represents an inertial coordinate system. With the geometry pictorially described, it can now be vectorized.

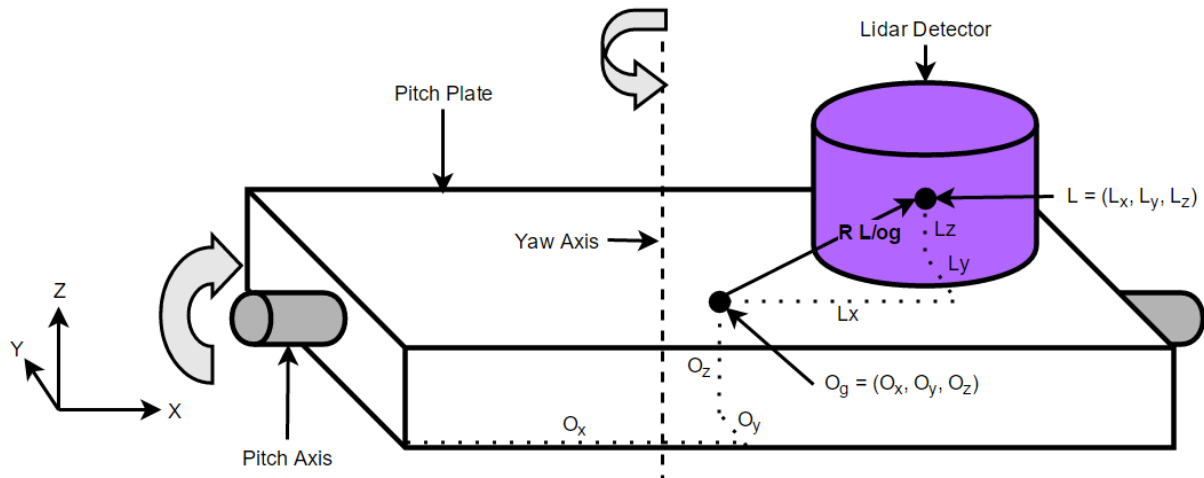


Figure 20: Pitch Plate Geometry

**B.3.1 Vectorized Geometry**

Fig. 21 depicts the vectorized dynamical system in a non-rotated configuration.

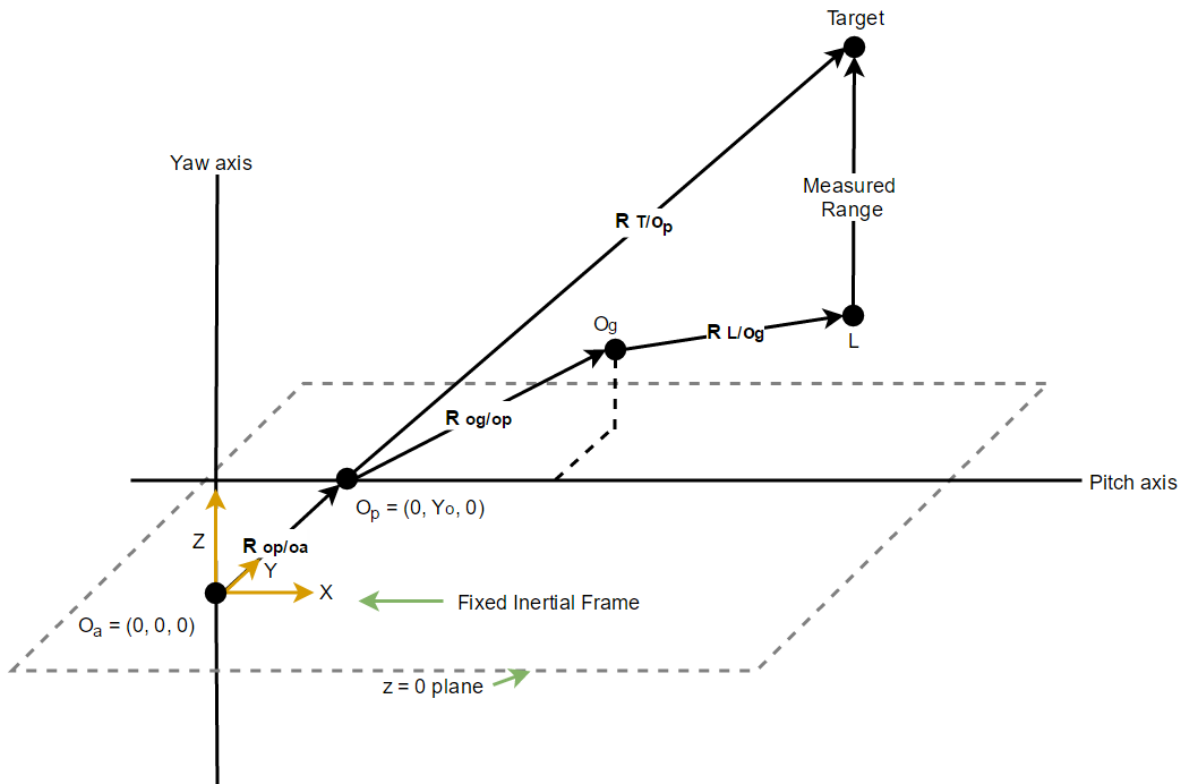


Figure 21: Vectorized Geometry

Note that the  $z = 0$  plane is defined as the  $xy$  plane that intersects both the pitch and azimuth axes, and that the pitch axis is aligned with the inertial  $x$  axis. The azimuth origin,  $O_a$  is defined as the point where the azimuth axis intersects the  $z = 0$  plane.  $O_a$  will serve as the absolute origin for our system. The pitch origin,  $O_p$ , is the point along the pitch

axis that is closest to  $O_a$ . The value of this distance is  $Y_o$ , and is only in the y direction as defined. We are actually free to select azimuth and pitch origins of rotation that are at any location along their respective axes, but placing them in this way simplifies the mathematics. The vector  $R_{T/O_a}$  is not shown, but is the ultimate objective. It is possible to determine the location of the pitch and azimuth axes relative to the geometric origin of pitch plate. This leads directly to the calculation of  $Y_o$ , and  $R_{O_g/O_p}$ , the position vector of the  $O_g$  with respect to  $O_p$ .  $R_{L/O_g}$  is the same vector from the previous section describing the location of the lidar detector with respect to  $O_g$ . The measured range will be defined as  $r$ , and is the distance from the lidar detector to some target. The vector  $R_{T/O_p}$  is the position of the target with respect to the pitch origin, and is simply the sum of  $R_{O_g/O_p}$ ,  $R_{L/O_g}$ , and  $r$ . In this and only this configuration  $R_{T/O_a}$  is the vector sum of  $Y_o$  and  $R_{T/O_p}$ . Rotation of both axes must now be accounted for in our vector sums to complete our definition of  $R_{T/O_a}$ .

### B.4 Definition of Co-rotating Frames

Fig. 22 gives the definition of the co-rotating frames that will be used to fully define  $R_{T/O_a}$  for any yaw and pitch angle. Firstly an inertial frame will be fixed at  $O_a$ . The azimuth frame will then also be fixed at  $O_a$  and initially aligned with the inertial frame. The azimuth frame is free to rotate about the inertial z axis. The pitch frame is fixed at the pitch origin, and is free to rotate about the  $X_p$  axis. Rotation of the azimuth axis also causes a physical translation of the pitch frame, causing a rotation of the pitch frame about the inertial z axis that is identical to the rotation of the azimuth frame.

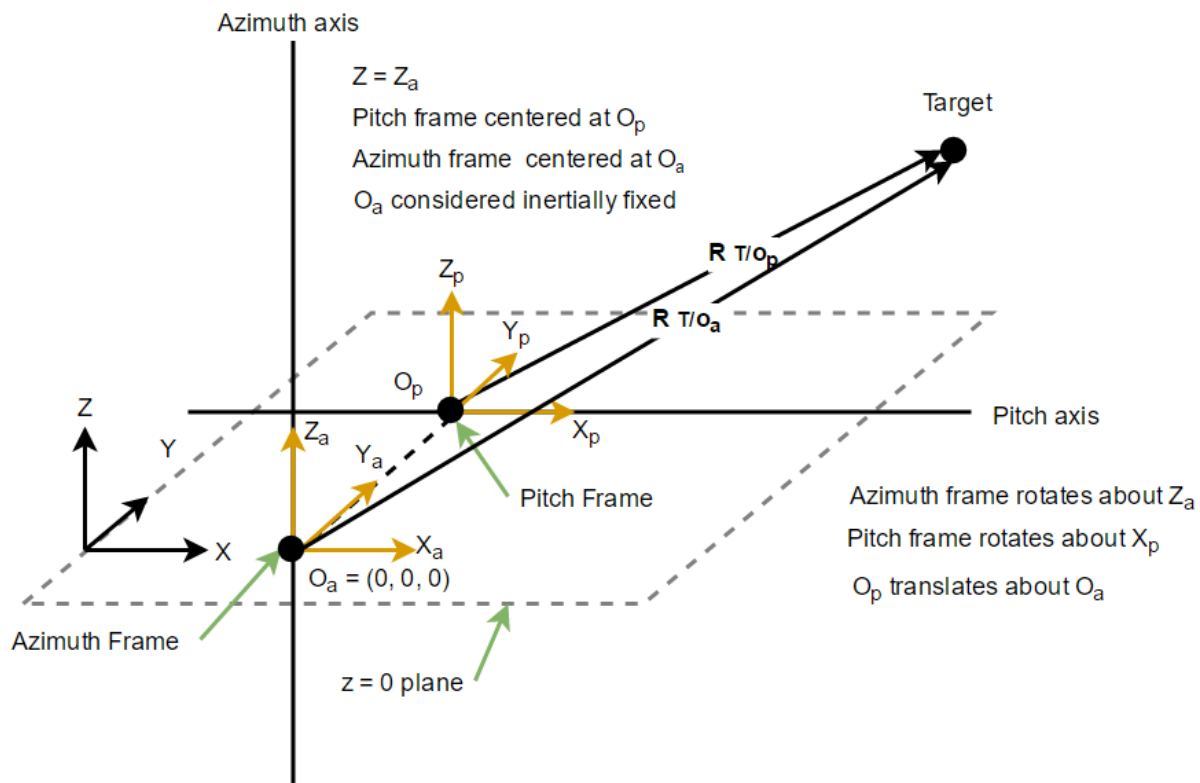
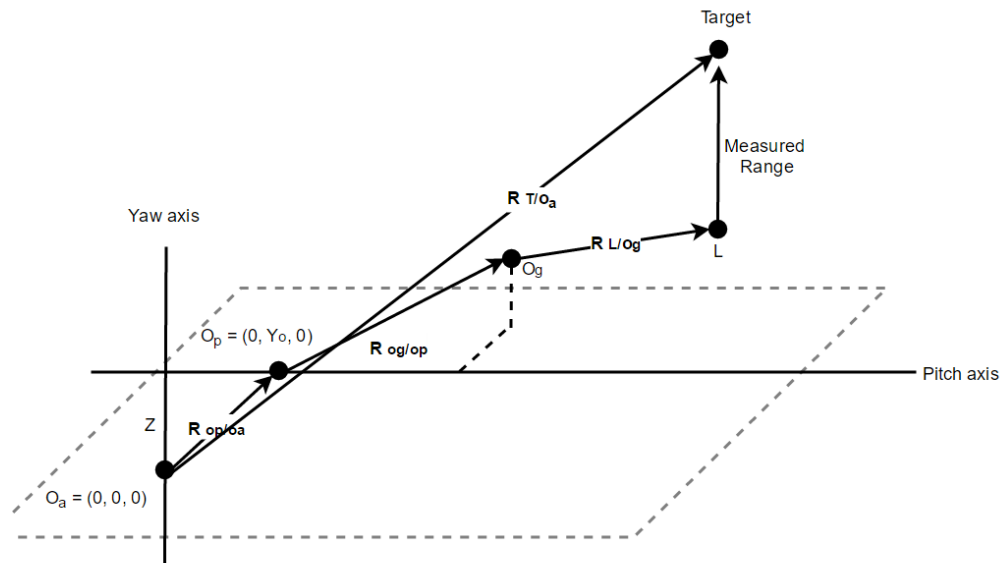


Figure 22: Co-rotating frames

### B.5 Derivation of Governing Equation

Derivation of  $R_{T/O_a}$  as a function of  $\phi$ ,  $\psi$ , and  $r$  is now simple using Euler angle rotations. The x, y, and z axes will be defined as the Euler 1, 2, and 3 axes respectively. Only two rotations will be required for our final result. Fig. 23

will serve as a reference for vector definitions. Recall that the azimuth and pitch frames are fixed to  $O_a$  and  $O_p$ , the azimuth and pitch origins, respectively.



**Figure 23:** Defined Vectors

$R_{T/O_p}$  in the pitch frame is only a function of the measured range  $r$ , and is given by equation 14.

$$[R_{T/O_p}]_p = [R_{O_g/O_p}]_p + [R_{L/O_g}]_p + [r]_p \quad (14)$$

$R_{T/O_p}$  expressed in the azimuth frame is equal to an Euler angle rotation about  $X_p$  of  $-\phi$ . Equation 15 captures this, where  $C_1(-\phi)$  is the matrix describing the rotation.

$$[R_{T/O_p}]_a = C_1(-\phi)[R_{T/O_p}]_p \quad (15)$$

We now have the position of the target relative to the pitch origin in the azimuth frame.  $R_{T/O_a}$  expressed in the azimuth frame is then the sum of  $[R_{T/O_p}]_a$  and  $Y_o$ . We must then express  $R_{T/O_a}$  in the inertial frame, which is done by rotating  $R_{T/O_a}$  by  $-\psi$  about the inertial  $z$  axis. Equation 16 gives  $R_{T/O_a}$  expressed in the inertial frame.

$$[R_{T/O_a}]_I = C_3(-\psi) \left( Y_o + [R_{T/O_p}]_a \right) \quad (16)$$

Equation 17 is the final result and gives  $[R_{T/O_a}]_I$  as a function of  $\phi$ ,  $\psi$ , and  $r$ .

$$[R_{T/O_a}]_I = C_3(-\psi) \left( Y_o + C_1(-\phi) \left( [R_{O_g/O_p}]_p + [R_{L/O_g}]_p + [r]_p \right) \right) \quad (17)$$

In conclusion the location of the target with respect to the pitch origin is first found and expressed in the pitch frame, and is only a function of the measured range. This vector is then rotated into the azimuth frame and summed with the offset distance of the pitch and azimuth origins. The result is then rotated into the inertial frame to obtain an inertial position vector from the azimuth origin to the target. The components of this vector are simply the  $x$ ,  $y$ , and  $z$  coordinates of the target with respect to the system origin. A point can be generated with these coordinates to indicate the location of the target, and carrying out this process over some raster of angular positions will result in the desired three dimensional map of some target area.

## C Hazard Detection and Definition

Exact calculation of the total uncertainty that would lead to 0.05 m cross range error yields  $0.188^\circ$ . Using  $0.15^\circ$  as the requirement gives margin to allow for both inaccuracy in provided specifications and design error. This is the absolute upper bound on the angular uncertainty of the return signal. The actual value in two dimensions depends on the elliptical spot projected onto the surface by the beam. However, this is a function of the surface being measured and will never be known to the system. As such the absolute maximum should be used to define the error.

### C.1 Shadowing

“Shadowing” occurs on the scanned terrain where the scanning pattern is blocked from reaching certain areas due to obstacles and rough terrain. This is an unavoidable problem when scanning from a point source, since any ray from the source to the ground can only travel by a direct, straight-line path. Shadowing can cause portions of the map to be completely hidden from the lidar, and so nothing can be assumed about the terrain in that location and so it must be assumed to be hazardous. The other effect of these obstacles and terrain is that points can become tightly clumped on the side facing the scan origin. Fig. 24 below demonstrates the effect of shadowing on a group of lidar scan lines in two dimensions.

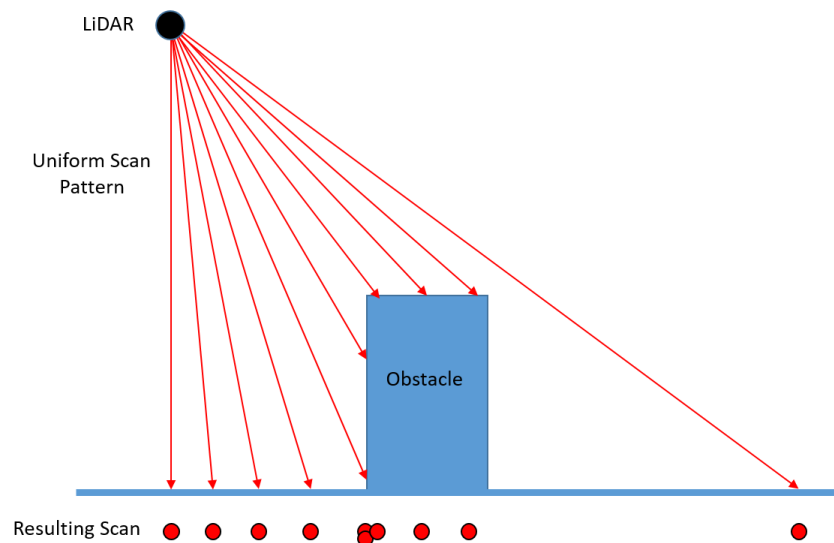


**Figure 24:** Two-Dimensional Shadowing Example

### C.2 Maximum Scan Angle

The effect of shadowing is a driving factor of the maximum angle that the system should deviate from nadir when scanning. The effects of shadowing become more drastic at larger angles, since obstacles block out an increasing amount of ground from the lidar’s view.

From a scan height of 15 meters above the ground plane, an obstacle of small height ( $\ll 15m$ ) will cast a shadow approximately equal to its angle away from the scan’s nadir line. This shadow cannot be completely mitigated, and so there must be an accepted potential for shadowing in the scan. The selected angle and rationale are defined in Section 2. Fig. 26 shows the effect of shadowing for up to  $20^\circ$  at the sides and approximately  $27^\circ$  at the corners. The white areas show regions where no scan points hit the terrain at those  $(x,y)$  positions. The shadowing starts to become severe at larger angles, where a section 36% of the height of the obstacle gets shadowed at a  $20^\circ$  scan angle and 51% of the height at a  $27^\circ$  scan angle. A maximum scan angle of  $20^\circ$  off of nadir was selected for a balance of achieving a large scan area without the shadowing having dominating effects on the scan.

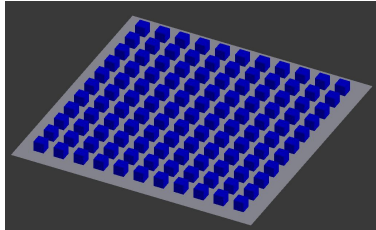


**Figure 25:** Blender scene to demonstrate shadowing

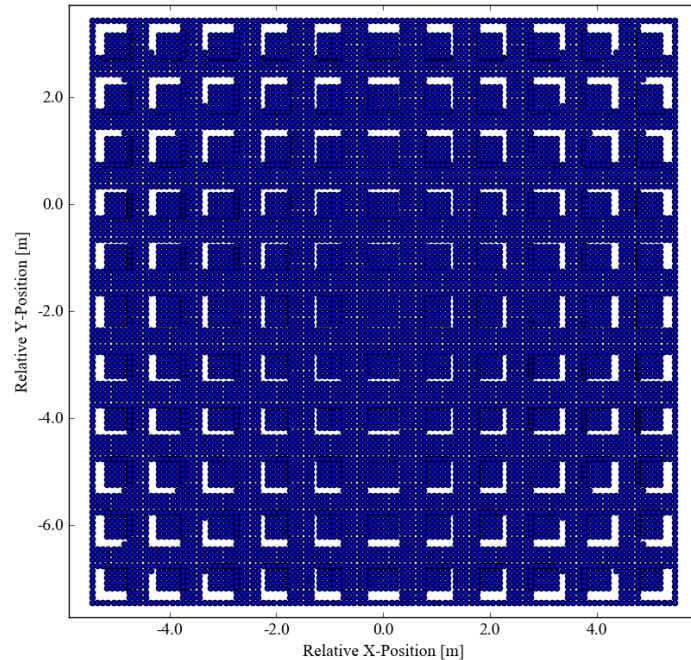


**Figure 26:** Ground-plane projection of scanned points

### C.3 Hazard Definition

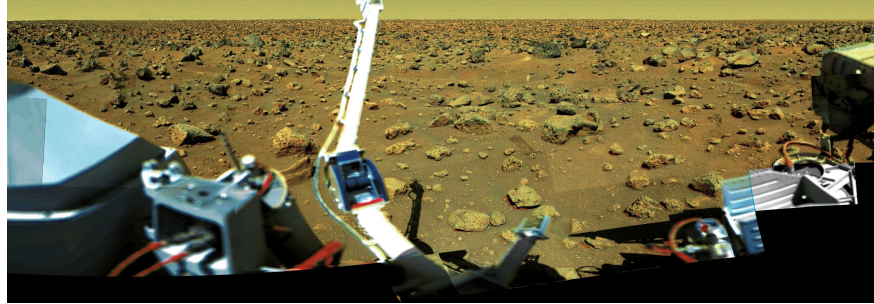
In order to define the obstacle or terrain dimensions that constitute a hazard, a few assumptions must be made about the lander's geometry and mission requirements:

1. The footprint of the lander with its landing legs deployed covers a  $0.5m \times 0.5m$  square.
2. The height of the lander body above the plane of the landing feet is  $15cm$ .
3. The lander cannot land more than  $15^\circ$  away from vertical.

Assumption 3 is taken from the landing requirement of the Curiosity rover for landing on slanted ground. It is then extrapolated to say that the lander cannot land on any surface that places it too far off-vertical. This then drives a definition of the height of an object considered a hazard, since the lander may land with one leg on the obstacle and the other legs on the ground. Using the  $50cm$  base width assumption, this defines the height of a hazard to be approximately  $13.4cm$ .

From this definition of hazard height, a lidar scan resolution can be derived under the premise that a certain percentage of obstacle hazards will go undetected. At this point, object detection becomes a probabilistic issue, where the distribution of object shapes will determine the detection rate from the scan.

To solve this problem, the aspect ratios of martian rocks can be used to model the distribution of ground objects. This can be extracted by taking the pixel aspect ratios of rocks from Mars satellite and rover pictures. Fig. 27 below was used to measure the shapes of 88 rocks from a side view. The measurements were taken as the pixel ratio of horizontal axis to vertical axis.



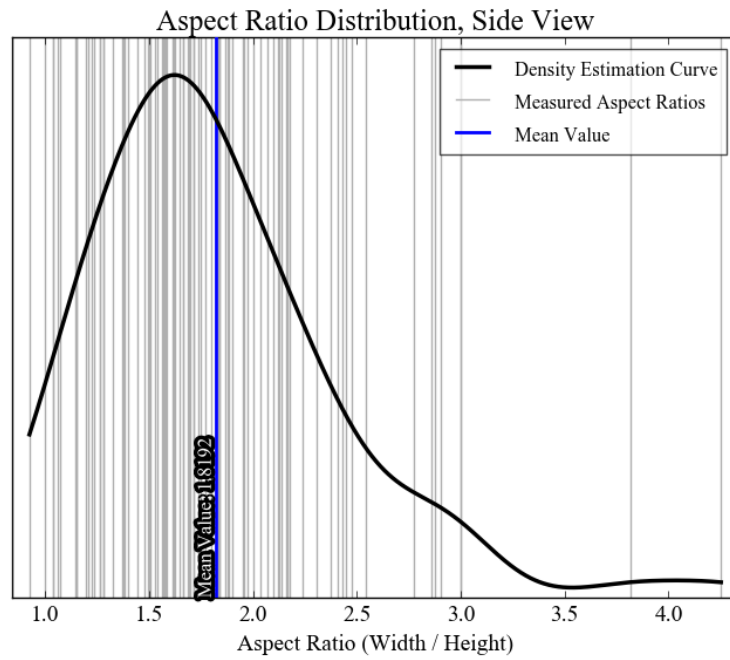
**Figure 27:** Martian Rocks from Side View

Fig. 28 below was used to measure the shapes of 65 rocks from a top view. The measurements were taken as the pixel ratio of long axis to perpendicular short axis. No assumption can be made in the side view picture about if the long axis or the short axis is facing the camera, so the top-view aspect ratios is assumed to have a median value of 1.0. Therefore, the measured aspect ratios (all  $\geq 1$ ) are inverted and included in the dataset.



**Figure 28:** Martian Rocks from Top View

The distribution of these values is calculated using a Gaussian Kernel Density Estimation, which creates a smoothed probability curve of what shape a rock is likely to be from each of these viewpoints. Fig. 29 shows this distribution for the side-view measurements, and Fig. 30 shows the distribution for the top-view measurements.



**Figure 29:** Distribution of Martian Rock Aspect Ratios, Side View

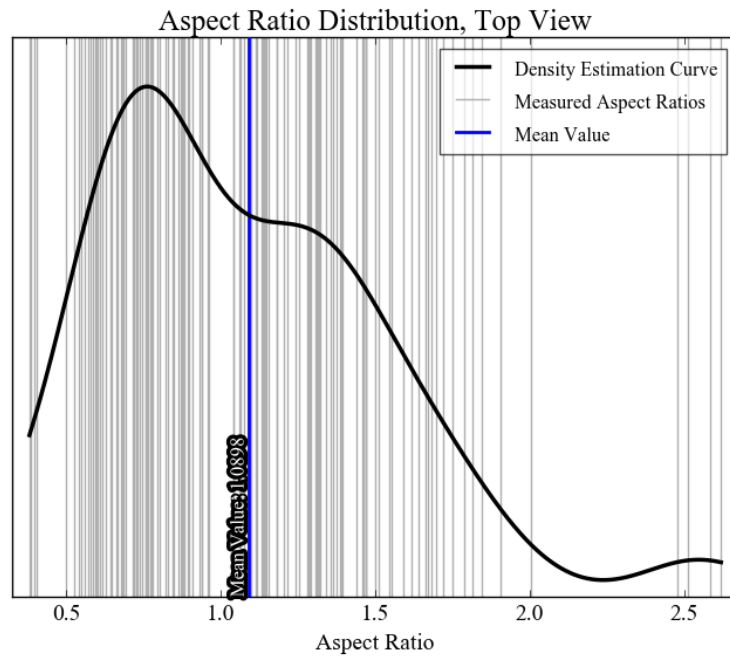


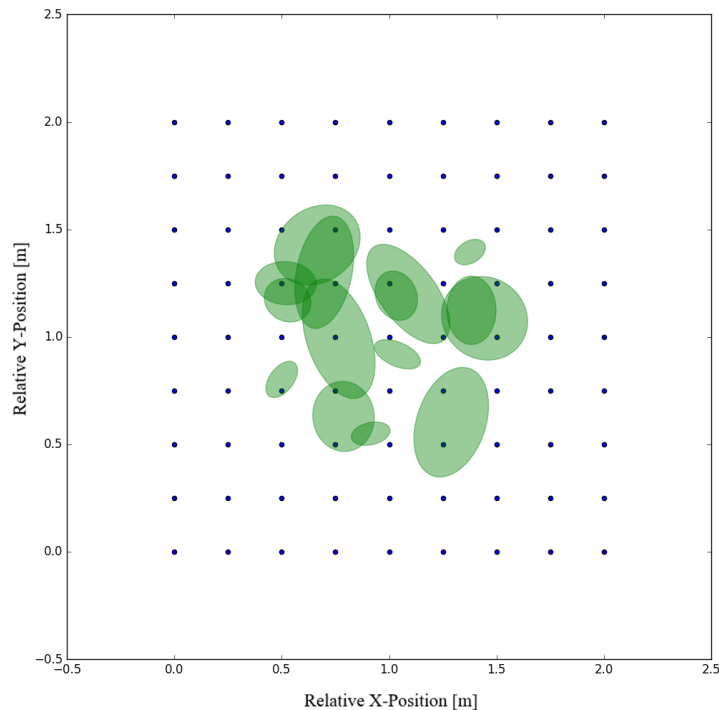
**Figure 30:** Distribution of Martian Rock Aspect Ratios, Top View

From these density estimation curves, the aspect ratios of rocks can be applied to a Monte Carlo simulation, where the shape and placement of rocks can be randomized and a scanning grid can be overlaid to see if any of the scan points overlap the rocks. The outcome of this analysis shows the likelihood of a realistically-shaped rock going undetected

by the scanning pattern. A few assumptions are made for this analysis:

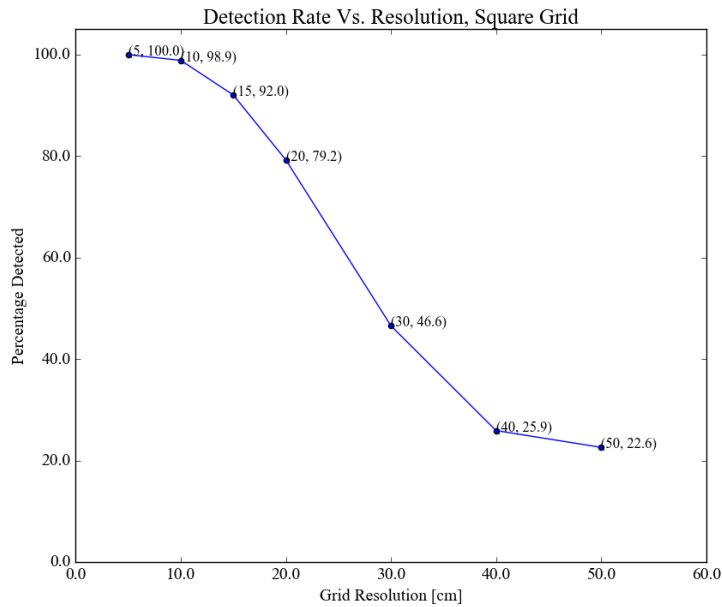
1. The height of all simulated rocks is the same, defined to be the hazard height of  $13.4\text{cm}$
2. The distribution of top-view aspect ratios follows the density estimation curve. shown in Fig. 30 and the side-view distribution follow the curve from Fig. 29.
3. Each rock can be modelled as an ellipsoid.
  - (a) The length dimension  $l$  can be defined as  $l = AR_s \times h$ , where  $AR_s$  is the side-view aspect ratio for the iteration of the Monte Carlo simulation, and  $h$  is the defined hazard height of  $13.4\text{cm}$ .
  - (b) The width dimension  $w$  can be defined as  $w = AR_t \times l$ , where  $AR_t$  is the top-view aspect ratio for the iteration of the Monte Carlo simulation.
4. The  $x$ - and  $y$ -locations (ground plane) of each rock are distributed uniformly over a  $1\text{m} \times 1\text{m}$  square.
5. The rotation of each rock is distributed uniformly between  $0^\circ$  and  $360^\circ$ .
6. The scanning grid spans a  $2\text{m} \times 2\text{m}$  square.
7. For each iteration, the rock counts as "detected" if any point of the scanning grid is contained within the top-down projection of the rock ellipsoid.

Fig. 31 below visualizes this technique for a small number of ellipsoid rocks, using a scan pattern of  $25\text{cm}$ .



**Figure 31:** Monte Carlo Simulation for Hazard Detection

This simulation was run with 10000 iterations for a uniformly distributed square scanning pattern, and a uniformly distributed equilateral triangle scanning pattern. The detection rates for the obstacles are shown for scanning resolutions of  $50\text{cm}$ ,  $40\text{cm}$ ,  $30\text{cm}$ ,  $20\text{cm}$ ,  $15\text{cm}$ ,  $10\text{cm}$ , and  $5\text{cm}$ . Fig. 32 shows the detection rate for the grid of squares, and Fig. 33 shows the detection rate for the equilateral triangle scan pattern.



**Figure 32:** Hazard Detection Rates for Square Grid Scan Pattern

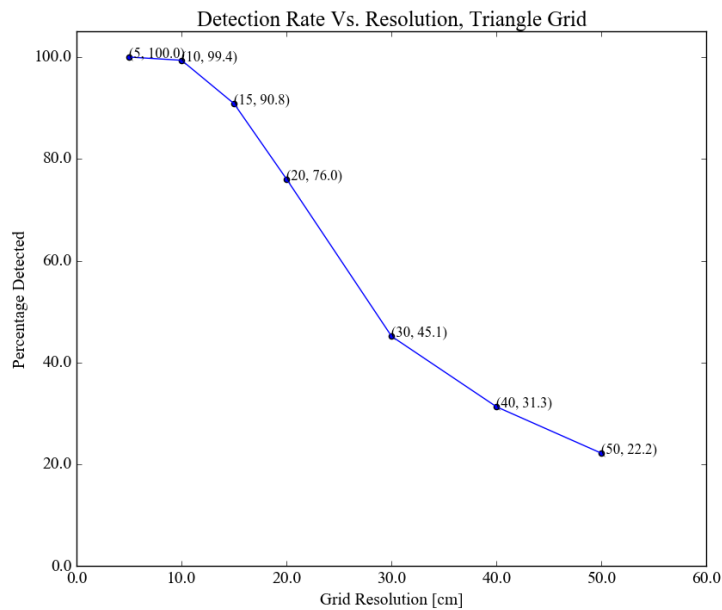


**Figure 33:** Hazard Detection Rates for Equilateral Triangles Scan Pattern

From this information, a specific spatial resolution requirement can be selected that properly balances hazard detection rate with mechanical demand on the system. 10cm is chosen as this balance, thus introducing a small, inherent risk to the system where there is an accepted risk of approximately 1.1% of a hazardous rock going undetected by a square scanning grid, and approximately 0.6% for the equilateral triangle scanning grid.

## D Stroking Neighbor Method

The Stroking Neighbor Method combines two well-known algorithms - stroking and the nearest neighbor method. Stroking is a procedure that extends the boundaries of a region by a set distance, which can be seen below in Figs. 34 & 35.



**Figure 34:** A binary image



**Figure 35:** A stroked version of the image, with the stroke shown in red

The stroking method will transform a binary hazard map (points designated either safe or hazardous) into a landing zone safety map, i.e. safe areas will represent points where the center of the landing site may be placed. As a visual aid, Fig. 36 is presented to confirm the validity of this approach.

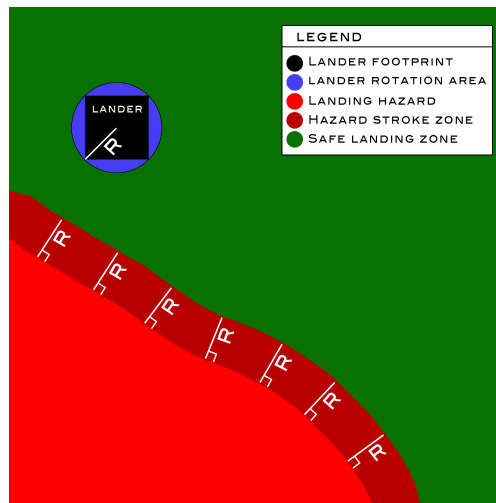


**Figure 36:** Motivation for the use of stroking to identify points for landing site center

On the original hazard map, the dark red band would have been deemed safe. Consider the circumscribing circle of the lander footprint shown in blue. Choosing this circle will allow the orientation of the lander footprint to be arbitrary. As this circle is brought tangent to the “landing hazard” zone (the *closest* it can be to the hazard region) the center of the lander footprint approaches a distance  $R$  from the hazard zone. Thus the center of the lander footprint may exist in the safe region excluding the original hazardous sites and the area stroked a distance  $R$  from those sites.

With this new hazard map that pertains not to the location of hazards, but rather to suitable sites for the center of the lander footprint, we invoke the Nearest Neighbor Algorithm. By taking the centroids of any hazard-free areas, we elect to choose the closest centroid to nadir and specify this as our landing site. Note that the algorithms for computing centroids of two-dimensional shapes in this setting have already been implemented by members of the group. Because we chose the circumscribing circle the lander may be rotated arbitrarily about its vertical axis. We

then send that location to the flight computer. The Nearest Neighbor approach is depicted visually below in Fig. 37. Nearest Neighbor algorithms are commonplace in computer science and implementation will pose no challenge.

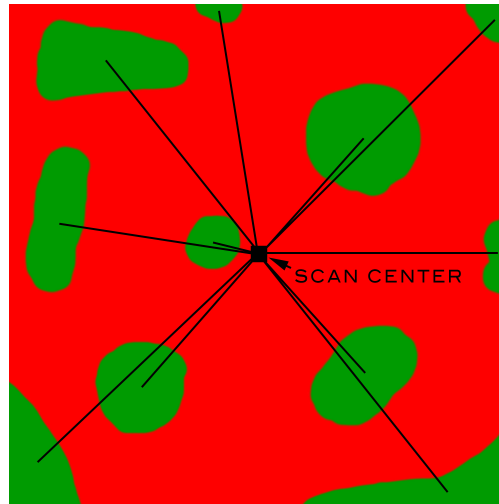


**Figure 37:** The closest centroid of a safe zone will be selected as a landing site center.

## E Algorithm Unit Test Maps

The robustness rating in Table 26 is weighted heavily but actual effectiveness of each of these algorithms is unclear without actually writing and testing the algorithms. Therefore, a series of “unit test” maps was defined in order to identify potential failure modes within the algorithm that can help distinguish the robustness of one method over another. The ranking in the table is determined by the number of unit tests for which these algorithms would theoretically be able to detect hazards properly. Fig. 38 - Fig. 42 show these unit test maps.

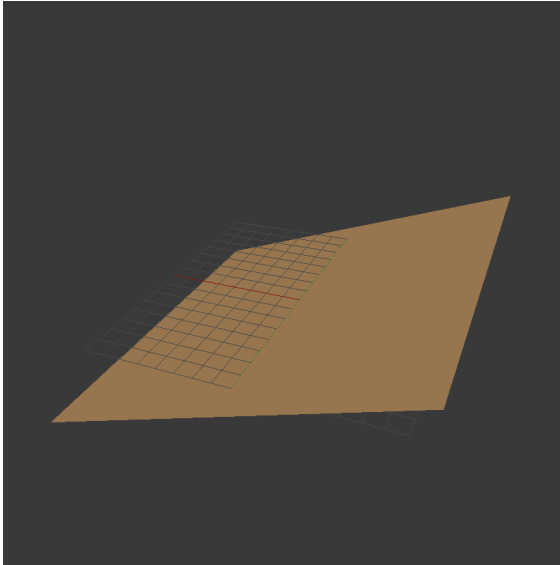


**Figure 38:** First unit test map: slanted plane with no obstacles

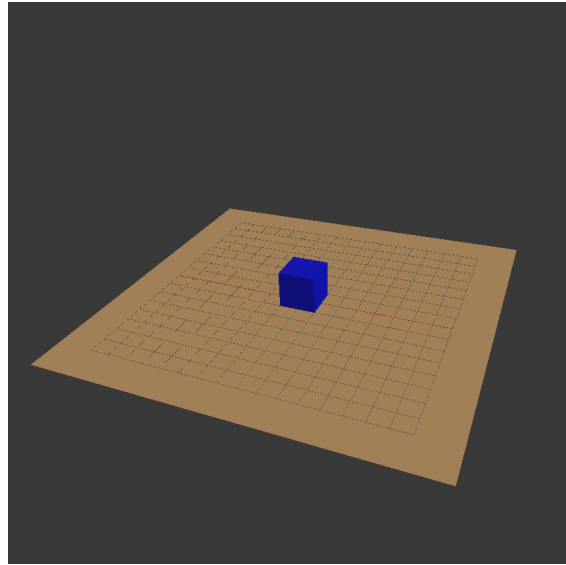


**Figure 39:** Second unit test map: flat plane with cube in center

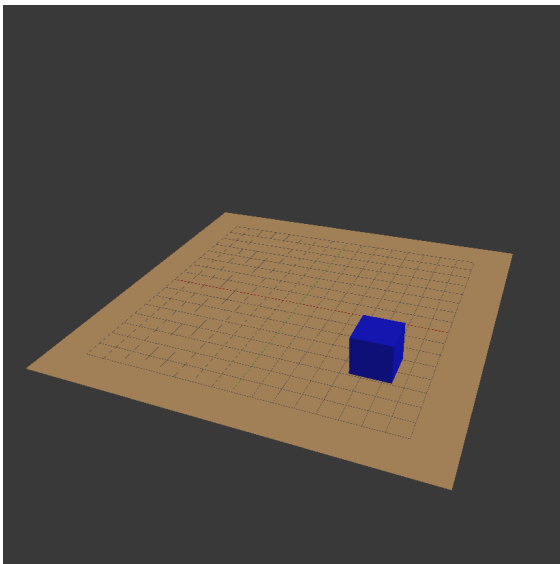


**Figure 40:** Third unit test map: flat plane with cube not in center

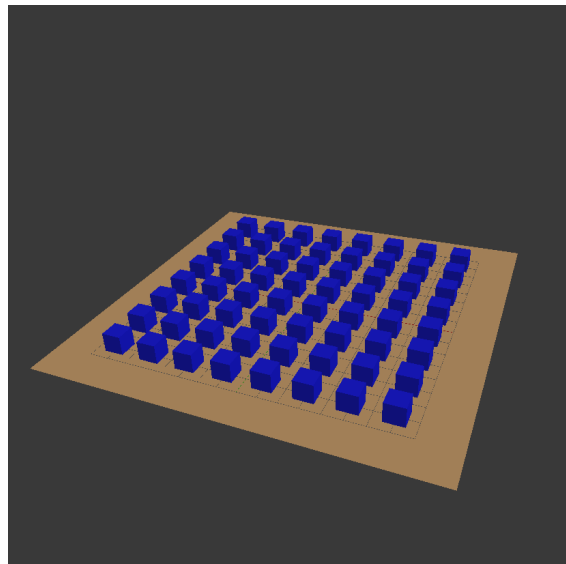


**Figure 41:** Fourth unit test map: flat plane with array of spaced cubes

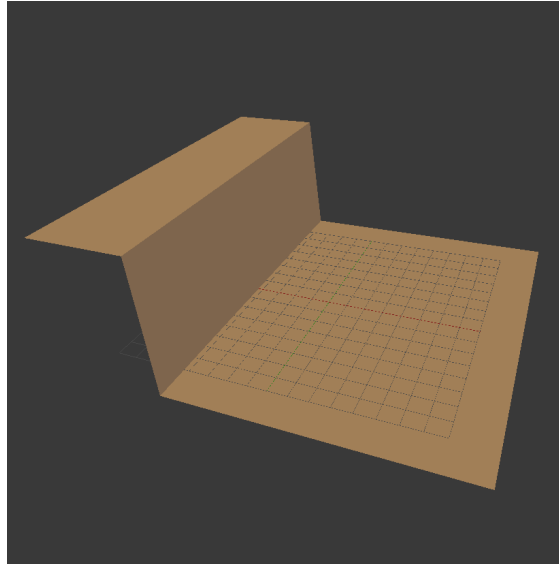


**Figure 42:** Fifth unit test map: cliff

Table 28: Algorithm Unit Test Results

	Failed Algorithms Per Unit Test
<b>Constant Slope</b>	<ul style="list-style-type: none"> <li>• <i>Simple Filter:</i> Only a band in the center will be reported as safe</li> </ul>
<b>Centered Cube</b>	<ul style="list-style-type: none"> <li>• <i>Simple Filter:</i> Cube top will be registered as ground level and everything else below it will be registered as hazardous</li> <li>• <i>Point Displacement:</i> The point displacement will be small at the edges of the cube since it is located close to nadir</li> </ul>
<b>Off-Center Cube</b>	<i>None</i>
<b>Spaced Array of Cubes</b>	<ul style="list-style-type: none"> <li>• <i>Surface-Based Filter:</i> The smoothed surface be wavy and the subtraction from the original surface will result in spikes and dips at all edges</li> <li>• <i>Fourier Decomposition:</i> Same issue as the Surface-Based filter</li> </ul>
<b>Cliff</b>	<ul style="list-style-type: none"> <li>• <i>Simple Filter:</i> Will not register the flat surface on the upper side of the cliff as safe</li> <li>• <i>Surface-Based Filter:</i> Half-passed. The smoothed surface will not capture the steepness of the cliff and so there will be zones near the cliff top and bottom that are not registered safe even though they are flat</li> <li>• <i>Fourier Decomposition:</i> Same rationale as the Surface-Based Filter</li> </ul>

## F Required Sample Rate Derivation

The required sample rate of the lidar sensor can be calculated from the nadir distance to local geoid, maximum scan angle, and spatial resolution. The maximum scan angle and spatial resolution were derived in Appendix C.2 and C.3. The nadir range to the local geoid can be directly calculated from the maximum scan angle and maximum slant range specified by the customer. The smallest possible scan area is a square where the corners are defined by the maximum scan angle of  $20^\circ$ . This square would have side lengths of  $7.25m$ . The required sample rate for a given spatial resolution is given by equation 18.

$$\text{Sample rate [Hz]} = \frac{\left(\frac{\text{Side Length}}{\text{Spatial Resolution}}\right)^2}{60} \quad (18)$$

Fig. 43 shows sample rate as a function of spatial resolution from  $0.04m$  to  $0.25m$ , and shows that not only is  $0.1m$  spatial resolution desired from a hazard detection perspective, but also from a required sample rate perspective. Spatial resolutions less than  $0.1m$  require quickly increasing sample rates, where as resolutions greater than  $0.1m$  require about sample rates that are decreasing slowly. This places  $0.1m$  right at the base of the smallest spatial resolution that can be achieved without requiring a comparatively large sample rate.

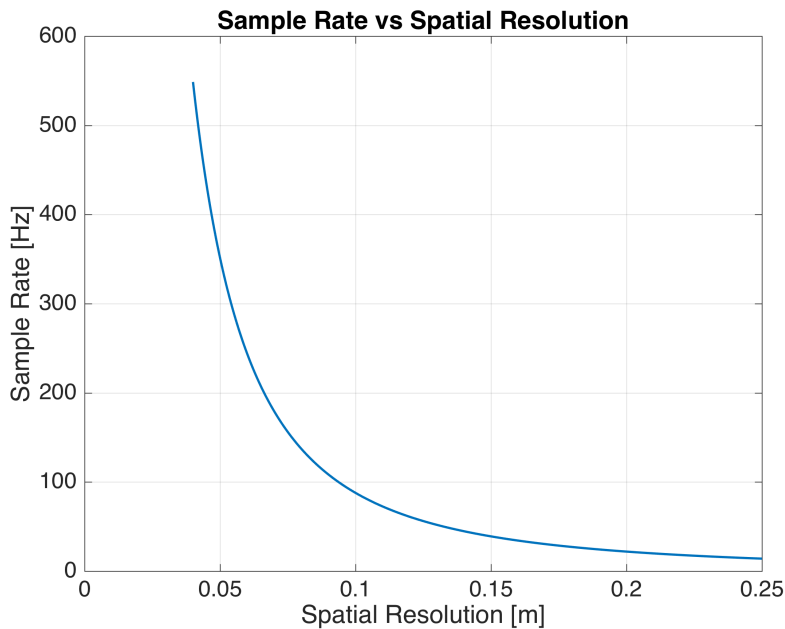


**Figure 43**

Although nadir range to the local geoid and maximum scan angle are already defined, their influence on required sample rate can be investigated. Fig. 44 and Fig. 45 show these sensitivity analyses. It is clear that at the specified scan angle of  $20^\circ$  and nadir geoid range of  $14.1m$  that required sample rate is not as sensitive as was the case for spatial resolution. Re-scoping these parameters will not have a significant impact on the required sample rate.

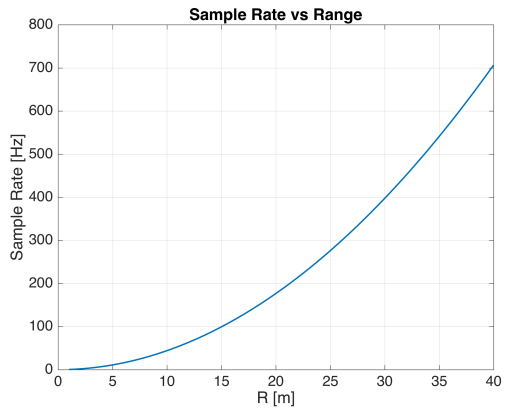


Figure 44

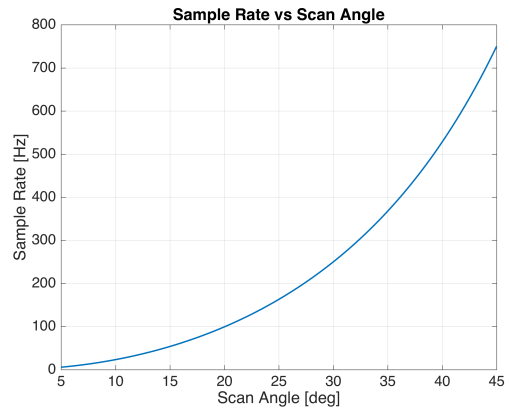


Figure 45